

# Loss of ZnT8 function protects against diabetes by enhanced insulin secretion

Om Prakash Dwivedi<sup>1#</sup>, Mikko Lehtovirta<sup>1#</sup>, Benoit Hastoy<sup>2#</sup>, Vikash Chandra<sup>3</sup>, Nicole A. J. Krentz<sup>4</sup>, Sandra Kleiner<sup>5</sup>, Deepak Jain<sup>6</sup>, Ann-Marie Richard<sup>7</sup>, Fernando Abaitua<sup>4</sup>, Nicola L. Beer<sup>2</sup>, Antje Grotz<sup>2</sup>, Rashmi B. Prasad<sup>8</sup>, Ola Hansson<sup>1,8</sup>, Emma Ahlqvist<sup>8</sup>, Ulrika Krus<sup>8</sup>, Isabella Artner<sup>8</sup>, Anu Suoranta<sup>1</sup>, Daniel Gomez<sup>5</sup>, Aris Baras<sup>5</sup>, Benoite Champon<sup>4</sup>, Anthony J Payne<sup>4</sup>, Daniela Moralli<sup>4</sup>, Soren K. Thomsen<sup>2</sup>, Philipp Kramer<sup>4</sup>, Ioannis Spiliotis<sup>2</sup>, Reshma Ramracheya<sup>2</sup>, Pauline Chabosseau<sup>9</sup>, Andria Theodoulou<sup>9</sup>, Rebecca Cheung<sup>9</sup>, Martijn van de Bunt<sup>2,4</sup>, Jason Flannick<sup>10,11</sup>, Maddalena Trombetta<sup>12</sup>, Enzo Bonora<sup>12</sup>, Claes B. Wolheim<sup>8</sup>, Leena Sarelin<sup>13</sup>, Riccardo C. Bonadonna<sup>14</sup>, Patrik Rorsman<sup>2</sup>, Benjamin Davies<sup>4</sup>, Julia Brosnan<sup>7</sup>, Mark I. McCarthy<sup>2,4,15</sup>, Timo Otonkoski<sup>3</sup>, Jens O. Lagerstedt<sup>6</sup>, Guy A Rutter<sup>9</sup>, Jesper Gromada<sup>4</sup>, Anna L. Gloyn<sup>2,4,15\*</sup>, Tiinamaija Tuomi<sup>1,13,16\*</sup> and Leif Groop<sup>1,8\*</sup>

1. Institute for Molecular Medicine Finland (FIMM), Helsinki University, Helsinki, Finland.
2. Oxford Centre for Diabetes Endocrinology & Metabolism, University of Oxford, UK.
3. Stem Cells and Metabolism Research Program and Biomedicum Stem Cell Centre, Faculty of Medicine, University of Helsinki, Finland.
4. Wellcome Centre for Human Genetics, University of Oxford, UK
5. Regeneron Pharmaceuticals, Tarrytown, New York, USA.
6. Department of Experimental Medical Science, Lund University, 221 84, Lund, Sweden.
7. Pfizer Inc, Cambridge, MA, United States of America.
8. Lund University Diabetes Centre, Department of Clinical Sciences, Lund University, Skåne University Hospital, SE-20502 Malmö, Sweden.
9. Section of Cell Biology, Department of Medicine, Imperial College London, Imperial Centre for Translational and Experimental Medicine, Hammersmith, Hospital, Du Cane Road, London, W12 0NN, UK.
10. Department of Molecular Biology, Massachusetts General Hospital, Boston, Massachusetts, USA.

11. Program in Medical and Population Genetics, Broad Institute, Cambridge, Massachusetts, USA.
12. Department of Medicine, University of Verona and Azienda Ospedaliera Universitaria Integrata of Verona, Verona, Italy
13. Folkhälsan Research Center, Helsinki, Finland.
14. The Azienda Ospedaliera Universitaria of Parma, 43125 Parma, Italy.
15. Oxford NIHR Biomedical Research Centre, Churchill Hospital, Oxford, UK
16. Abdominal Center, Endocrinology, Helsinki University Central Hospital; Research Program for Clinical and Molecular Metabolism, University of Helsinki, Helsinki, Finland.

# These authors contributed equally to the study

\* These authors jointly supervised this study

*Correspondence:* Leif Groop, Institute for Molecular Medicine Finland (FIMM), Helsinki University. Leif.

[Groop@helsinki.fi](mailto:Groop@helsinki.fi) and/or [leif.Groop@med.lu.se](mailto:leif.Groop@med.lu.se)

68    **Abstract**

69    A rare loss-of-function allele p.Arg138\* in *SLC30A8* encoding the zinc transporter 8 (ZnT8),  
70    enriched in Western Finland, protects against type 2 diabetes (T2D). We recruited relatives of the  
71    identified carriers and showed that protection was associated with better insulin secretion due to  
72    enhanced glucose responsiveness and proinsulin conversion, particularly when compared with  
73    individuals matched for the genotype of a common T2D-risk allele in *SLC30A8*, p.Arg325. In  
74    genome-edited human iPSC-derived  $\beta$ -like cells, we establish that the p.Arg138\* allele results in  
75    reduced *SLC30A8* expression due to haploinsufficiency. In human  $\beta$ -cells, loss of *SLC30A8* leads to  
76    increased glucose responsiveness and reduced  $K_{ATP}$  channel function similar to isolated islets from  
77    carriers of the T2D-protective allele p.Trp325. These data position ZnT8 as an appealing target for  
78    treatment aimed at maintaining insulin secretion capacity in T2D.

79

80 Zinc transporters (ZNT) regulate the passage of zinc across biological membranes out of the  
81 cytosol, while Zrt/Irt-like proteins (ZIP) transport zinc into the cytosol<sup>1</sup>. ZnT8, encoded by  
82 *SLC30A8*, is highly expressed in the membrane of insulin granules within pancreatic  $\beta$ -cells, where  
83 it transports zinc ions for crystallization and storage of insulin<sup>2</sup>. We previously described a loss-of-  
84 Function (LoF) allele p.Arg138\* (rs200185429, c.412C>T) in the *SLC30A8* gene that conferred  
85 53% protection against T2D<sup>3</sup>. This allele was extremely rare (0.02%) in most European countries  
86 but more common (>0.2%) in Western Finland<sup>3</sup>. We also reported a protective frameshift allele  
87 p.Lys34Serfs50\* conferring 83% protection against T2D in Iceland<sup>3</sup>. Further, the *SLC30A8* gene  
88 harbors a common variant (rs13266634, c.973T>A) p.Trp325Arg in the C-terminal domain<sup>4</sup>. Whilst  
89 the major p.Arg325 allele (>70% of the population) confers increased risk for T2D, the minor  
90 p.Trp325 allele is protective<sup>5</sup>.

91 The mechanisms by which modulation of ZnT8 activity protects against T2D are largely unknown.  
92 Several attempts have been made to study loss of *Slc30a8* function in rodent models, but the results  
93 have been inconclusive; global knock-out of *Slc30a8* led to either glucose intolerance or had no  
94 effect in mice<sup>6,7,8</sup>, whilst over-expression improved glucose tolerance without effect on insulin  
95 secretion<sup>9</sup>. A mouse model harboring the equivalent of the human p.Arg138\* allele lacked any  
96 detectable ZnT8 protein but showed no effect on glucose tolerance<sup>10</sup>. These rodent studies present a  
97 complex picture that may not recapitulate the T2D protective effects of *SLC30A8* LoF alleles in  
98 humans. We therefore performed detailed metabolic studies in human carriers heterozygous for the  
99 LoF allele (p.Arg138\*) recruited on the basis of their genotype, performed comprehensive  
100 functional studies in human  $\beta$ -cell models, and compared these with the mouse model carrying the  
101 human p.Arg138\*-*Slc30a8* allele.

102

103

## 104    **Results**

### 105    **Recruitment by genotype**

106    Given the enrichment of the p.Arg138\*-*SLC30A8* allele in Western Finland, we genotyped >14,000  
107    individuals from the Botnia Study<sup>11</sup> for the *SLC30A8* p.Arg138\* and the common p.Trp325Arg  
108    variants, and identified 71 p.Arg138\*-*SLC30A8* carriers (all heterozygotes; 55 non-diabetic  
109    individuals, Fig. 1). We then recruited family members of known p.Arg138\* carriers to identify  
110    additional p.Arg138\* carriers to perform a detailed metabolic study (190 minutes test meal) in  
111    carriers and non-carrier relatives. Of the 79 p.Arg138\* carriers (65 novel, 14 previously identified)  
112    and 103 non-carrier relatives from >21 families (Supplementary Fig. 1), 54 and 47, respectively,  
113    participated in a test meal and 31 and 13 participated in an oral glucose tolerance test (OGTT)  
114    during a separate second visit (Fig. 1, Supplementary Table 1 and 3). We also had data from  
115    previously performed OGTTs within the Botnia Study for 8436 non-diabetic individuals (55  
116    p.Arg138\* carriers, Fig. 1, Supplementary Table 2 and 3). Of the 136 p.Arg138\* allele carriers,  
117    none were homozygous for the protective common variant, p.Trp325, and p.Arg138\* segregated  
118    with p.Arg325 in all families (Supplementary Fig. 1). Thus, we present the data in three different  
119    ways: 1) p.Arg138\* vs. all p.Arg138Arg, 2) p.Arg138\* vs. p.Arg138Arg having at least one  
120    p.Arg325 allele (p.Trp325Arg or p.Arg325Arg), and 3) p.Arg325 (p.Trp325Arg or p.Arg325Arg)  
121    vs. p.Trp325Trp on a background of p.Arg138Arg.

122    Replicating our previous findings<sup>3</sup>, carriers of p.Arg138\* had a reduced risk of T2D (OR=0.40,  
123    p=0.003) when analyzing 4564 T2D (13 p.Arg138\* carriers) and 8183 non-diabetic (55 p.Arg138\*  
124    carriers) individuals. Additionally, non-diabetic p.Arg138\* carriers had lower fasting glucose  
125    concentrations than p.Arg138Arg individuals (Supplementary Table 5 and 6). There were no  
126    significant differences in plasma zinc concentrations measured during test meal or OGTT between  
127    the groups (data not shown).

128 *Comparison of p.Arg138\* vs. p.Arg138Arg*: The p.Arg138\* carriers had lower blood glucose levels  
129 during the test meal especially during the first 40 minutes ([area under curve](#),  $p=0.02$ ) and showed a  
130 higher corrected insulin response (CIR) (at 20 minutes,  $p=0.046$ ) than non-carriers ([Supplementary](#)  
131 [Tables 4](#)). Similarly, in the larger population-based OGTT cohort, carriers had higher insulin  
132 response during OGTT (Fig 3b-c, left panel), especially with respect to the early incremental insulin  
133 response ( $p=0.008$ ) and the insulin/glucose ratio (at 30 minutes,  $p=0.002$ , [Supplementary Table 5](#)).  
134 [The higher insulin secretory response during OGTT was consistent across different subsets with](#)  
135 [OGTT data \(meta-analysis: CIR,  \$P=0.002\$ ; incremental insulin,  \$p=2.4\times 10^{-4}\$ ; 30 minutes insulin,](#)  
136  [\$p=3.8\times 10^{-4}\$ \) \(Supplementary Table 6\).](#) Of note, the p.Arg138\* carriers had significantly lower  
137 proinsulin/C-peptide (20 minutes:  $p=0.041$ ; 40 minutes:  $p=0.043$ ) and proinsulin/insulin (20  
138 minutes:  $p=0.006$ ) ratios during the test meal suggesting effects on proinsulin conversion (Fig. 2d-  
139 e). No differences were seen in glucagon, GLP-1 or free fatty acid concentrations during the test  
140 meal ([Supplementary Fig. 2c-e](#)). Neither model-based insulin clearance index nor the ratio of  
141 insulin and C-peptide areas under the curve during the test meal differed between p.Arg138\* and  
142 p.Arg138Arg ([Supplementary Fig. 2f-g](#)).

143 *Comparison of p.Arg138\* vs. p.Arg138Arg–p.Arg325*: The above differences were magnified when  
144 we restricted the p.Arg138Arg group to carriers of the common risk variant p.Arg325 (middle panel  
145 of Fig. 2). The early phase (0-40 minutes) insulin ( $p=0.026$ ), insulin/glucose ratio ( $p=0.004$ ) and  
146 CIR ( $p=0.004$ ; 20 minutes) were all greater in p.Arg138\* carriers vs. p.Arg138Arg on a background  
147 of p.Arg325 ([Supplementary Table 4](#)). Both the proinsulin/C-peptide (20 minutes:  $p=0.027$ , 40  
148 minutes:  $P=0.044$ ) and proinsulin/insulin ratios (20 minutes:  $P=0.003$ ) were reduced in p.Arg138\*  
149 carriers (middle panel of Fig. 2d-e).

150 *Comparison of p.Trp325Trp vs. p.Arg325*: The effect of p.Trp325Trp genotype on glucose and  
151 insulin response mimicked the effects of p.Arg138\* with pronounced early (20 minutes) insulin  
152 ( $p=0.032$ ) and C-peptide ( $p=0.030$ ) responses during the test meal (right panel of Fig. 2b-c and

Supplementary Fig. 2a), as well as increased insulin secretion (30 minutes insulin, 30 minutes insulin/glucose, incremental insulin,  $p \leq 0.003$ ), lower fasting and 120 minute proinsulin ( $p = 0.006$  and  $p = 0.039$ , respectively) concentration during OGTT in p.Trp325 carriers (Supplementary Table 5, right panel of Fig. 3b-c). Moreover, p.Trp325Trp carriers showed a pronounced increased ( $p = 0.003$ ) early incremental insulin secretion during the intravenous glucose tolerance test (IVGTT) (Supplementary Fig. 3a-b and Supplementary Table 5). In patients with newly diagnosed T2D (Supplementary Table 7), the p.Trp325Trp carriers showed a trend ( $p = 0.12$ ) towards enhanced  $\beta$ -cell sensitivity to glucose during the OGTT (Supplementary Fig. 3c).

Taken together, all human *in vivo* data on p.Arg138\* show enhanced glucose-stimulated insulin secretion combined with enhanced proinsulin conversion as a potential explanation for T2D protection. The common allele p.Trp325 is also associated with protection from T2D and the metabolic effects are similar but more modest than those of on p.Arg138\*, suggesting it also might reduce ZnT8 function.

#### ***SLC30A8* p.Arg138\* and p.Lys34Serfs50\* variant in human iPSCs**

The majority of nonsense *SLC30A8* alleles (including p.Arg138\* and p.Lys34Serfs50\*) which protect against T2D are located in the first four exons of the eight-exon canonical islet *SLC30A8* transcript (ENST00000456015) and are predicted to undergo nonsense mediated decay (NMD), a cell surveillance pathway that reduces errors in gene expression by eliminating mRNA transcripts with premature stop codons. To confirm that nonsense *SLC30A8* alleles lead to haploinsufficiency through NMD, we used CRISPR-Cas9 to introduce two protective alleles, p.Arg138\* and p.Lys34Serfs50\*, into the *SLC30A8* locus of the SB Ad3.1 human iPSC cell line (Supplementary Fig. 4a). Two heterozygous hiPSC lines for the *SLC30A8*-p.Arg138\* allele (clone B1 and A3) and two homozygous hiPSC lines for *SLC30A8*-p.Lys34Serfs50\* (clone B3 and D3) were generated and compared with an unedited wildtype and a CRISPR-Sham hiPSC line. All hiPSC lines passed quality control checks including karyotyping and pluripotency (Supplementary Fig. 4b-c).

178 We subjected our *SLC30A8*-edited iPSCs to a previously published *in vitro* endocrine pancreas  
179 differentiation protocol<sup>12</sup> (Supplementary Fig. 4). At the end of the seven stage protocol, *SLC30A8*  
180 expression was significantly reduced in cells heterozygous for the p.Arg138\* allele (clone A3  
181  $0.06\pm0.03$ ,  $p<0.0001$ ; clone B1  $0.04\pm0.01$ ,  $p<0.0001$ ) or homozygous for the p.Lys34Serfs50\*  
182 (clone B3  $0.04\pm0.01$ ,  $p<0.0001$ ; clone D3  $0.04\pm0.01$ ,  $p<0.0001$ ) compared to unedited control cells  
183 ( $1.02\pm0.13$ ) (Fig. 4a). In addition, ZnT8 protein was absent in homozygous p.Lys34Serfs50\*  
184 hiPSC-derived beta-like cells compared to wildtype controls, but was also undetectable in  
185 differentiated heterozygous p.Arg138\* clones (Fig. 4b-c), suggesting an impact on differentiation.  
186 Indeed, the number of *INS*- and *SLC30A8*-transcript expressing cells were reduced in clones with  
187 premature stop codons in *SLC30A8* (Supplementary Fig. 4d-g), indicating a reduced formation of  
188 beta-like cells. To disentangle effects on differentiation from those on expression, allele-specific  
189 *SLC30A8* expression was quantified by digital droplet PCR<sup>13</sup> in the heterozygous p.Arg138\* lines.  
190 Of note, p.Arg138\* allele-specific *SLC30A8* expression was reduced compared to the WT allele  
191 (clone A3:  $24.3\pm3.1\%$ ,  $p<0.0001$ ; clone B1:  $22.2\pm1.7\%$ ,  $p<0.0001$ ) (Fig. 4d). The reduced  
192 expression of the mutant *SLC30A8* allele (clone A3:  $18.2\pm1.8\%$ ; clone B1:  $18.6\%$ ;) compared to the  
193 wildtype allele ( $81.7\pm1.3\%$ ) was confirmed ( $p<0.0001$ ) by targeted *SLC30A8* mRNA sequencing  
194 (Fig. 4e and Supplementary Fig. 5c). Although not statistically significant inhibition of NMD by  
195 cycloheximide showed a trend towards a greater rescue of the p.Arg138\* transcript compared to the  
196 p.Arg138Arg transcript (clone A3:  $230\pm61\%$  vs.  $150\pm33\%$ ,  $p=0.28$  and clone B1:  $198\pm45\%$  vs.  
197  $152\pm26\%$   $p=0.39$ , Fig. 4f-g). Taken together, these data show that the protective p.Arg138\*-  
198 *SLC30A8* allele undergoes NMD, resulting in haploinsufficiency for *SLC30A8*.

### 199 **Impact of *SLC30A8* loss in a human $\beta$ -cell line**

200 Since human *in vivo* studies provided strong evidence for a role of the p.Arg138\* on insulin  
201 secretion and proinsulin processing, we studied the impact of *SLC30A8* loss using siRNA mediated  
202 knock down (KD) on both phenotypes in a well characterized human  $\beta$ -cell model EndoC- $\beta$ H1<sup>14</sup>.



203 By siRNA, we achieved a 30-65% decrease in *SLC30A8* mRNA levels ( $p \leq 0.003$ , Fig. 5a,  
 204 Supplementary Fig. 7a) which resulted in reduced ZnT8 protein levels (Fig. 5b) associated with a  
 205 reduction in intracellular zinc content (34%,  $p = 0.002$ ) (Fig. 5c). Assessment of dense core granule  
 206 zinc content in *SLC30A8*-silenced EndoC- $\beta$ H1 cells (Supplementary Fig. 6a), through the use of the  
 207 cell surface attached fluorescent zinc probe ZIMIR<sup>15</sup> (Supplementary Fig. 6b-c) revealed a tendency  
 208 ( $p = 0.10$ , Supplementary Fig. 6d), for reduced Zn<sup>2+</sup> release, consistent with the loss of zinc from this  
 209 compartment, and also with previous findings in islets from *Slc30a8* null mice<sup>15</sup>.

210 KD of *SLC30A8* had no significant effect on stimulated insulin secretion neither in response to 20  
 211 mM glucose nor to the sulphonylurea tolbutamide (which closes K<sub>ATP</sub> channels) (Fig. 5d). However,  
 212 basal insulin secretion was significantly increased in si*SLC30A8* transfected cells ( $p = 0.048$ ) and the  
 213 inhibitory effect of diazoxide, a K<sub>ATP</sub> channel opener, on glucose-stimulated insulin secretion, was  
 214 significantly reduced ( $p = 8 \times 10^{-3}$ , Fig. 5d). There was no effect of *SLC30A8* KD on insulin content  
 215 (Fig. 5e). We then measured the resting membrane conductance ( $G_m$ ) in si*SLC30A8* transfected  
 216 cells incubated with 100  $\mu$ M diazoxide (to activate K<sub>ATP</sub> channels). In control cells,  $G_m$  was in  
 217 agreement with previous reports<sup>16</sup>, while *SLC30A8* KD reduced  $G_m$  by 65% ( $p = 0.002$ , Fig. 5f)  
 218 without altering cell size (Fig. 5g). Indeed, reduced K<sub>ATP</sub> channel activity is consistent with the  
 219 reduced expression observed of the genes encoding the K<sub>ATP</sub> channel subunits, SUR1 (*ABCC8*) and  
 220 Kir6.2 (*KCNJ11*) ( $P = 0.04$  and  $0.06$  respectively, Fig. 5h). In addition, insulin secretion elicited by  
 221 the combination of elevated 50mM extracellular K<sup>+</sup> ( $[K^+]_o$ ) to depolarize the cells and open voltage-  
 222 gated Ca<sup>2+</sup> channels and 16.7 mM glucose was significantly higher after *SLC30A8* KD ( $p = 0.002$ ,  
 223 Fig. 5i). The proinsulin-insulin ratios (both total and secreted hormones) and proinsulin  
 224 concentrations were decreased in si*SLC30A8* transfected cells ( $p \leq 0.007$  and  $\leq 0.018$  respectively,  
 225 Fig. 5j-k), but no differences in either protein or mRNA levels of genes (*PCSK1*, *PCSK2* and *CPE*)  
 226 involved in proinsulin processing in *SLC30A8* KD cells was observed (Fig. 5m-p, Supplementary

Fig. 7a). However, we did observe increased AKT phosphorylation (pAKT-473) and improved cell survival under ER stress ( $p=0.016$  and  $0.016$  respectively, Fig. 5q-s) in *SLC30A8* KD cells.

We next examined the effects of *SLC30A8* KD on gene expression in EndoC- $\beta$ H1 cells by mRNA sequencing (RNA-seq) of si*SLC30A8* treated and siScramble cells ( $n=8$  vs.  $8$ ). We observed a total of 674 significantly differently expressed genes among 12,956 protein coding genes that passed the quality control filters (Supplementary Fig. 7 and Supplementary Data Set 1). RNA-seq confirmed the reduction in *KCNJ11* and *ABCC8* expression in *SLC30A8* KD cells ( $p=2.6 \times 10^{-18}$  and  $p=2.04 \times 10^{-9}$  respectively, Supplementary Fig. 7c) as seen earlier by qPCR (Fig. 5h). In addition, further genes involved in the regulation of  $\beta$ -cell excitability/exocytosis, including *CACNA1C*, were up-regulated in KD cells (Supplementary Fig. 7c). Moreover, expression of genes associated with  $\beta$ -cell maturation and development were also influenced by *SLC30A8* KD with decreased expression of *NKX6.1* and *PDX1* and increased expression of *SOX4*, *SOX6* and *SOX11* (Supplementary Fig. 7b). A pathway enrichment analysis of differentially expressed genes revealed enrichment of genes involved in the WNT signaling and insulin secretion pathways (Supplementary Fig. 7 and Supplementary Data Set 1). A global gene set enrichment analysis (GSEA) of all expressed genes ( $N=12,956$ ) using a gene ontology database revealed enrichment of genes involved in positive regulation of TOR signaling (Supplementary Fig. 7) in KD cells. Collectively, these data demonstrate a link between *SLC30A8* expression and transcriptional networks involved in cell development, cell fate and plasma membrane polarization.

#### Metabolic phenotype of mice carrying the human *SLC30A8* p.Arg138\*

Since neither global nor tissue specific *Slc30a8* KO mouse models have recapitulated the human phenotype in carriers of the *SLC30A8* p.Arg138\* allele, we attempted to overcome this problem by using a mouse model carrying the human *Slc30a8* p.Arg138\* allele<sup>10</sup>. On a standard chow diet there was no evidence of enhanced insulin secretion<sup>10</sup> but when subjected to a high fat diet (HFD) the mice showed a significant increase in insulin secretion ( $p<0.01$ , Fig. 6i), and similar changes in

252 proinsulin/insulin ( $p=0.0004$ ) and proinsulin/C-peptide ratios ( $p<0.0001$ ) as seen in human carriers  
253 (Fig. 6f-g). No significant changes were seen in insulin clearance, glucose or insulin tolerance (Fig.  
254 6h, j, k).

#### 255 **Impact of p.Arg138\* on protein localization and cytosolic zinc distribution in INS-1 cells**

256 Although we found no evidence for the presence of a truncated protein in the human p.Arg138\*  $\beta$ -  
257 cell model (Fig. 4) as also reported for the p.Arg138\* mice<sup>10</sup>, we still explored the possibility that a  
258 truncated protein could result from mRNA evading NMD. Transient overexpression of tagged  
259 ZnT8-p.Arg138\* fusion protein in a rat insulinoma cell line, INS-1e, showed distinct punctate  
260 distribution patterns, consistent with localization of the truncated ZnT8 protein to secretory  
261 granules, as previously observed with the full length protein<sup>17</sup> (Supplementary Fig. 8a-c).  
262 Additionally, Western blot showed stable expression of truncated ZnT8 in native INS1e cells  
263 (Supplementary Fig. 8d).

264 To investigate the effects of a truncated ZnT8 protein on cytosolic free  $Zn^{2+}$ , we used a genetically-  
265 encoded  $Zn^{2+}$  sensor eCALWY-4<sup>18</sup>. Overexpression of the truncated protein (p.Arg138\*,  
266 Supplementary Fig. 8e-f) had no impact on cytosolic free  $Zn^{2+}$  when expressed in INS-1(832/13)  
267 cells (Supplementary Fig. 8g).

#### 268 **Influence of common *SLC30A8* variants p.Trp325Arg in primary human islets**

269 Although we were unable to study the effects of the rare T2D-protective alleles in primary human  
270 islets we were able to assess the impact of the p.Trp325Arg genotype on *in vitro* insulin and  
271 glucagon secretion. Islets obtained from cadaveric p.Trp325 carriers secreted more insulin  
272 ( $p=0.0153$ ) than p.Arg325Arg carriers when stimulated with high glucose (16.7 mM) and  
273 depolarizing  $[K^+]_o$  (70 mM) in line with findings of *SLC30A8* KD in EndoC- $\beta$ H1 (Fig. 7a-b).  
274 Interestingly, a trend towards increased glucose responsiveness was already observed at  
275 submaximal glucose stimulation (6 mM) (Fig. 7c). Increasing glucose from 1 mM to 6 mM

stimulated insulin secretion 2.2 ( $p=0.031$ ) and 2.7 ( $p=0.012$ ) fold in p.Arg325 and p.Trp325 carriers respectively, with no effect on insulin content (Fig. 7c-d).

As *SLC30A8* is highly expressed in human alpha cells<sup>1</sup>, we also measured glucagon secretion from the same islets (Fig. 7e-f). In islets from p.Arg325Arg donors, 6 mM glucose inhibited glucagon secretion by ~50% compared to 1 mM glucose. In islets from p.Trp325Arg donors, glucagon secretion at 1 mM glucose was reduced by 50% ( $p=0.033$ ) compared to p.Arg325Arg donors with no effect on glucagon content (Fig. 7e-f).

Finally we explored co-expression of *SLC30A8* with relevant candidate genes (*INS*, *GCG*, proinsulin processing and  $K_{ATP}$  channel subunits) as well as the impact of p.Trp325Arg on their expression (Fig. 7g-j). *SLC30A8* transcript levels showed strong positive correlation with expression of all candidate genes (*GCG*,  $p \leq 1.3 \times 10^{-7}$ , *PCSK1*,  $p \leq 1.5 \times 10^{-7}$ , *PCSK2*,  $p \leq 4.6 \times 10^{-10}$ , *CPE*,  $p \leq 3.2 \times 10^{-6}$ , *KCNJ11*,  $p \leq 7.1 \times 10^{-7}$ , and *ABCC8*,  $p \leq 1.6 \times 10^{-11}$ ) except *INS*. The protective p.Trp325 allele showed a trend (non-significant) of decreased *SLC30A8* expression ( $p=0.053$ ) as well as genes involved in proinsulin processing such as *PCSK1* ( $p=0.041$ ), *PCSK2* ( $p=0.045$ ) and *ABCC8* ( $p=0.049$ ).

Taken together, these data suggest that the common T2D-protective allele (p.Trp325) may also improve the response to a glucose challenge (Fig. 2 and Fig. 3) by enhancing insulin secretion and possibly by reducing glucagon secretion in primary human islets.

**Discussion**

The current study demonstrates the strengths of using human models for studying the consequences of variants associated with human diseases. Although over 30 T2D protective LoF or missense alleles in *SLC30A8* have been reported<sup>19</sup>, previous studies in rodents<sup>6, 17, 20, 21, 22</sup>, have failed to provide a mechanistic explanation for the protection. This human study robustly shows that enhanced insulin responsiveness to glucose, combined with enhanced proinsulin processing,

300 contribute to the protection from T2D. As all LoF carriers had the common risk p.Arg325 allele on  
301 the same haplotype, the effect of the LoF allele was most evident when compared against p.Arg325  
302 carriers emphasizing the importance of considering the genetic background of human LoF carriers.

303 In our human iPSC derived beta-like cells, two different LoF alleles (p.Arg138\* and  
304 p.Lys34Serfs50\*) show a clear reduction in *SLC30A8* expression, suggesting that NMD induced  
305 haploinsufficiency is likely a common mechanism for rare LoF alleles in *SLC30A8*. Although a  
306 recent study showed increased zinc transporter activity for the common risk variant p.Arg325<sup>23</sup>, it  
307 should be kept in mind that the common p.Trp325Arg locus is complex as another 3' UTR variant  
308 (rs3802177) is in strong linkage disequilibrium with p.Trp325Arg. This variant (rs3802177) may  
309 potentially affect *SLC30A8* transcription/translation, further modulating the effect of p.Trp325Arg  
310 on ZnT8 function.

311 Interestingly, in our human iPSC based model of *SLC30A8* LoF mutations (p.Arg138\* and  
312 p.Lys34Serfs50\*), loss of ZnT8 protein decreased the formation of *INS*<sup>+</sup> cells. In support of this, we  
313 observed decreased expression of multiple genes associated with beta cell development (including  
314 *PDX1*) and changes in expression of genes involved in WNT signaling (including *TCF7L2*) after  
315 partial ZnT8 loss (KD) in the human EndoC- $\beta$ H1 cell line. However, insulin content was not  
316 affected suggesting that partial ZnT8 loss is unlikely to affect beta-cell development. In support of  
317 this, complete ZnT8 null mice were viable with preserved beta-cell function<sup>6,9,10</sup>. We have not been  
318 able to examine this in humans as we did find any human homozygous for *SLC30A8* LoF alleles.

319 Whilst data from all our sub-studies are consistent with increased insulin secretion, the precise  
320 molecular mechanisms for the involvement of zinc and zinc transporters remain elusive.

321 Data derived from the human  $\beta$ -cell line show a clear decrease in intracellular zinc content and a  
322 trend towards a reduction in co-secreted granular zinc after ZnT8 loss. These observations are  
323 consistent with previous rodent studies demonstrating that loss of ZnT8 function reduces total islet

324 zinc content (including R138\* mice<sup>10</sup>) as well as free Zn<sup>2+</sup> in the cytosol and granules<sup>6,9,17,24</sup>. The  
325 LoF p.Arg138\* and p.Lys34Serfs50\* alleles in humans are likely to exert similar effects on  
326 intracellular and granular zinc concentrations. In the present study over-expression of the truncated  
327 p.Arg138\* protein in INS-1 cells did not result in changes in cytosolic zinc concentrations which is  
328 consistent with haploinsufficiency. In contrast, a recent human study showed that the T2D risk  
329 p.Arg325 allele was associated with higher islet zinc concentrations<sup>25</sup>. In support of a potential role  
330 for zinc in the development of diabetes, Zn<sup>2+</sup> plays an important role as regulator of cellular  
331 excitability<sup>26</sup> in the CNS. In beta-cells Zn<sup>2+</sup> induced inhibition of L-type voltage-gated Ca<sup>2+</sup>  
332 channels could result in inhibition of insulin secretion<sup>27</sup>, whilst, Zn<sup>2+</sup> has been reported to directly  
333 activate K<sub>ATP</sub> channel currents<sup>28</sup>. The down regulation of the K<sub>ATP</sub> channel subunits genes following  
334 *SLC30A8* knockdown suggests that there is coordinated expression of these genes. It is therefore  
335 tempting to hypothesize that *SLC30A8* expression may contribute to the normal K<sub>ATP</sub> channel  
336 density in both  $\beta$  and  $\alpha$  cells but this remains to be demonstrated. The combined consequence of  
337 a reduction in K<sub>ATP</sub> channel gene expression and a reduction in para/autocrine electrophysiological  
338 regulation (on calcium and K<sub>ATP</sub> channels activities) by Zn<sup>2+</sup> could contribute to enhanced insulin  
339 secretion as well as reducing glucagon secretion at low glucose levels. Indeed, a similar effect on  
340 alpha cells secretory capacity has been observed upon inhibition of K<sub>ATP</sub> channel activity using  
341 tolbutamide<sup>29</sup>.  
342 Zn<sup>2+</sup> is essential for proper insulin crystallization, and loss of ZnT8 results in reduced dense core  
343 granules and increased granule diameter possibly due to more non-crystalline insulin which is  
344 expected to be released rapidly during exocytosis<sup>6,17,30</sup>. The increased basal insulin secretion seen in  
345 the human  $\beta$ -cell line following *SLC30A8* KDs and also reported in islets from *Slc30a8* null mice<sup>17</sup>  
346 who also display impaired insulin crystallization, suggests that there is preferential release of non-  
347 crystalline insulin. It has also been suggested that increased insulin clearance could explain the  
348 decrease in circulating insulin concentrations<sup>20</sup>. However, we did not find any support for changes

349 in insulin clearance in human p.Arg138\* carriers or p.Arg138\* mice on HFD, nor did we see any  
350 effect on the incretin hormone GLP-1 in humans.

351 In contrast to the consistent effect of human p.Arg138\* and p.Trp325Arg on proinsulin processing,  
352 studies in mice following the loss of ZnT8 have reported inconsistent effects on proinsulin  
353 processing, ranging from inhibitory effects<sup>20,21</sup> to beneficial effects in transgenic Trp325Arg mice  
354 on HFD<sup>22</sup>. The reasons for this remain unclear but since blocking of the insulin receptor prevents  
355 the positive effect on insulin processing in R138\* mice<sup>10</sup>, it is possible that insulin receptor  
356 signaling modulates the effect of loss of ZnT8 on proinsulin processing.

357 The most reproducible finding in all sub-studies of *SLC30A8* loss was enhanced glucose-stimulated  
358 insulin secretion associated with increased conversion of proinsulin to C-peptide and insulin.

359 Carriers of the p.Trp325 T2D protective allele also showed a similar phenotype consistent with  
360 previous published studies reporting impaired proinsulin conversion in carriers of the risk p.Arg325  
361 allele<sup>31,32</sup>. It has been suggested that it takes some time for insulin to mature and become  
362 biologically active<sup>33,34</sup>. It is therefore possible that the pronounced effect of the LoF T2D-  
363 protective allele at 20 and 40 minutes of the test meal could reflect an effect on the time-course of  
364 insulin maturation.

365 Our study has both strengths and limitations. Among its strengths are the comprehensive studies in  
366 humans recalled by their genotype in a region of the world where the p.Arg138\* allele is enriched.  
367 The complementary studies in both human cell lines as well as the humanized mice can also be  
368 considered as a strength. A limitation is the inconclusive measurements of zinc in different cellular  
369 compartments and characterization of insulin granule cargo. This part will require the development  
370 of better intracellular sensors of zinc which will enable these studies in the future.

371 In conclusion, our data consistently demonstrate that heterozygosity for a LoF allele p.Arg138\* and  
372 homozygosity for a common allele p.Trp325Trp of *SLC30A8* are associated with increased insulin  
373 secretion capacity and a lower risk of developing T2D and in the absence of any on-target adverse

374 [events](#). Therefore, ZnT8 remains an appealing safe target for antidiabetic therapies preserving  $\beta$ -cell  
375 function.

## 376 **Online Methods**

### 377 **Human study population**

378 The Botnia Study has been recruiting patients with T2D and their family members in the area of  
379 five primary health care centers in western Finland since 1990. Individuals without diabetes at  
380 baseline (relatives or spouses of patients with T2D) have been invited for follow-up examinations  
381 every 3-5 years<sup>11</sup>. The Prevalence, Prediction and Prevention of diabetes (PPP)–Botnia Study is a  
382 population-based study in the same region including a random sample of 5,208 individuals aged 18  
383 to 75 years from the population registry<sup>38</sup>. Diabetes Registry Vaasa (DIREVA) is regional diabetes  
384 registry of > 5000 diabetic patients from Western Finland (Botnia region)<sup>39</sup>. In the current study, we  
385 included >14,000 individuals (Botnia family study=5678, PPP=4862, and DIREVA=3835). All  
386 participants gave their written informed consent and the study protocol was approved by the Ethics  
387 Committee of Helsinki University Hospital, Finland (the Botnia studies) and the Ethics Committee  
388 of Turku University Hospital (DIREVA).

### 389 ***Oral Glucose Tolerance Test (OGTT, [Fig. 3](#)) and test meal ([Fig. 2](#) and [Supplementary Fig. 2](#)):***

390 Subjects maintained a weight-maintaining diet and avoided vigorous exercise for 3 days prior to the  
391 OGTT or test meal, which were performed after an overnight fast. Height, weight, hip and waist  
392 circumferences, fat percentage (%; bioimpedance analyzer) and blood pressure (sitting, 3  
393 measurements after 5 minutes rest) were measured. The participants ingested 75 g dextrose (in a  
394 couple of minutes, OGTT) or a 526 kcal mixed meal (in 10 minutes, test-meal: 76 g carbohydrate,  
395 17 g protein and 15 g fat). Blood samples were drawn from an antecubital vein for plasma (P-) glucose  
396 and serum (S-) insulin and C-peptide at 0, 30, 120 minutes during the OGTT; for P-glucose,  
397 P-glucagon, S- insulin, S-C-peptide, S-zinc, and total S-GLP-1 at 0, 20, 40, 70, 100, 130, 160 and



190 minutes during the test meal. Test meal samples for S-FFA were collected at 0, 40 and 120 minutes and for S-proinsulin at 0, 20, 40 and 130 minutes, respectively. Urine was collected between 0 – 70 and 70 – 190 minutes for the determination of glucose and zinc excretion during the test meal.

**Intravenous Glucose Tolerance Test (IVGTT, [Supplementary Fig. 3](#)):** IVGTT group consists of total 849 (male- 403, female- 446) individuals with an average age of 51 years. An antecubital polyethylene catheter was placed to one hand for the infusion of 0.3 g/kg body weight of glucose (maximum dose 35 g) intravenously for 2 minutes. A retrogradely positioned wrist vein catheter was placed in the other hand, held in a heated (70°C) box in order to arterialize the venous blood. Arterialized blood samples were drawn at 0, 2, 4, 6, 8, 10, 20, 30, 40, 50 and 60 minutes for P-glucose and S-insulin.

**Biochemical measurements ([Fig. 2, 3](#) and [Supplementary Fig. 3a-b](#)):** P-glucose was analyzed using glucose oxidase (Beckman Glucose Analyzer, Beckman Instruments, Fullerton, CA, USA; Botnia Family Study) or glucose dehydrogenase method (Hemocue, Angelholm, Sweden; PPP-Botnia and test meal studies). In the Botnia Family study, S-insulin was measured by radioimmunoassay (RIA, Linco; Pharmacia, Uppsala, Sweden), enzyme immunoassay (EIA; DAKO, Cambridgeshire, U.K.) or fluoroimmunometric assay (FIA, AutoDelfia; Perkin Elmer Finland, Turku, Finland). For the analysis, insulin concentrations obtained with different assays were transformed to cohere with those obtained using the EIA. The correlation coefficient between RIA and EIA as well as between FIA and EIA was 0.98 ( $P < 0.0001$ ). S-insulin was measured by the FIA in baseline visit of PPP-Botnia and the test meal study (correlation co-efficient 0.98). S-proinsulin was measured using RIA (Linco; Pharmacia, Uppsala, Sweden, OGTT data) or EIA (Mercodia AB, Uppsala, Sweden; test-meal data), and P-glucagon using RIA (EMD Millipore, St. Charles, MO; OGTT data) or EIA (Mercodia AB, Uppsala, Sweden; test-meal data). S-FFA was measured by an enzymatic colorimetric method (Wako Chemicals, Neuss, Germany). Serum total

cholesterol, HDL and triglyceride concentrations were measured with Cobas Mira analyzer (Hoffman LaRoche, Basel, Switzerland), and since 2006 with an enzymatic method (Konelab 60i analyser; Thermo Electron Oy, Vantaa, Finland). Serum LDL cholesterol was calculated using the Friedewald formula. Blood collected in tubes containing DPP4-inhibitors was used for radioimmunoassay<sup>40</sup> for total P-GLP-1 (intact GLP-1 and the metabolite GLP-1 9-36 amide) during test meal.

Serum and urine samples for zinc were collected in trace element tubes (Beckton Dickinson, NJ, USA) and S- and U-zinc analyzed by two commercial laboratories: NordLab (Oulu, Finland; atom absorption spectrophotometry, AAS) until 6<sup>th</sup> May 2015, then in Synlab (Helsinki, Finland; AAS for serum, mass spectrophotometry ICP-MS for U-zinc). The S-zinc concentrations were corrected for P-albumin (r=0.34, p=0.008 for Nordlab, r=0.34, p=0.03 for Synlab).

Corrected insulin response (CIR) was calculated for test meal (at 20 minutes) and OGTT (at 30 minutes) using the formula  $CIR(t) = Ins(t) \cdot 100 / [Gluc(t) \cdot (Gluc(t) - 3.89)]$ , where Ins(t) and Gluc(t) are insulin (in mU/L) and glucose concentrations (in mmol/L) at sample time point (minutes)<sup>41</sup>.

Estimation of Insulin clearance index was done on the model based estimation of glucose-, insulin- and C-peptide curves during the test meal using the equation  $AUC_{ISR} / [AUC_{ins} + (I_{basal} - I_{final}) \cdot MRT_{ins}]$ , where  $AUC_{ISR}$  is the area under the curve of insulin secretion rate,  $AUC_{ins}$  is the area under the curve of insulin concentration,  $I_{final}$  is insulin concentration at the end, and  $I_{basal}$  insulin concentration at the beginning of the study<sup>42</sup>.  $MRT_{ins}$  is the mean residence time of insulin, and was assumed to be 27 minutes as reported previously<sup>43</sup>.

**Genotyping:** We analyzed genotype data for rs13266634 (p.Trp325Arg) and rs200185429 (p.Arg138\*) for three cohorts genotyped with different genome-/exome-wide chips: the Botnia family cohort (Illumina Global Screening array-24v1, genotyped at Regeneron Pharmaceuticals), PPP-Botnia (Illumina HumanExome v1.1 array, genotyped at Broad Institute) and DIREVA (Illumina Human CoreExome array-24v1, genotyped at LUDC). For the Botnia family cohort,

448 genotype data for p.Arg138\* were imputed (info score >0.95) from the available GWAS data by  
449 phasing using SHAPIT v2<sup>44</sup> and imputing using the GoT2D reference panel<sup>45</sup> by IMPUTEv2<sup>46</sup>.  
450 The carrier status of all 20 imputed p.Arg138\* from Botnia family cohort was additionally  
451 confirmed from available exome sequencing data. Genotyping (p.Trp325Arg and p.Arg138\*) the  
452 family members participating in the genotype based recall study (test meal study) was performed  
453 using TaqMan (Applied Biosystems, Carlsbad, CA) and additionally genotyped by Illumina Global  
454 Screening array-24v1. The genotype distribution of both variants was in accordance with Hardy-  
455 Weinberg equilibrium in all the cohorts. We did not detect any Mendelian errors in the families.

456 **Genetic Association Analysis:** All the quantitative traits were inversely normally transformed  
457 before the analyses. The family-based recall study included only non-diabetic subjects during test  
458 meal. Association analysis of rare p.Arg138\* with glycemic indices obtained during family-based  
459 recall test meal study (left and middle panel of Fig. 2 , Supplementary Fig. 2 and Supplementary  
460 Table 4) was performed using family-based association analyses (orthogonal model together with  
461 100,000 Monte-Carlo permutations) adjusting for age, sex, BMI, and additionally other covariates  
462 (genotype of p.Trp325Arg for middle panel only) as implemented in QTDT (v2.6.1)<sup>35</sup>. Association  
463 analysis of common p.Trp325Arg with glycemic indices obtained during family-based recall test  
464 meal study (right panel of Fig. 2 , Supplementary Fig. 2, and Supplementary Table 4) was  
465 performed using QFAM family-based association test with 100,000 permutations to correct for any  
466 family structure as implemented in PLINK<sup>36</sup> (--qfam-total, --mperm 100,000). The association  
467 analysis of p.Arg138\* and p.Trp325Arg with glycemic traits during OGTT studies including only  
468 non-diabetic individuals (Fig. 2 , Supplementary Table 5 and Supplementary Table 6) and IVGTT  
469 (Supplementary Fig. 3) was performed using mixed linear model considering genetic relatedness  
470 among samples as implemented in GCTA (v1.91)<sup>37</sup>. The fixed-effects meta-analysis of all OGTT  
471 studies (Supplementary Table 6) were performed using METAL software package<sup>47</sup>. The linear  
472 mixed model (adjusting for genetic relatedness) also used for T2D association analysis.

473 ***Study participants and their clinical measurements in the Verona Newly Diagnosed Diabetes***

474 ***Study (VNDS, [Supplementary Fig. 3c](#)):*** The Verona Newly Diagnosed Type 2 Diabetes Study  
475 (VNDS; NCT01526720) is an ongoing study aiming at building a biobank of patients with newly  
476 diagnosed (within the last six months) type 2 diabetes. Patients are drug-naïve or, if already treated  
477 with antidiabetic drugs, undergo a treatment washout of at least one week before metabolic tests are  
478 performed<sup>48</sup>. Each subject gave informed written consent before participating in the research, which  
479 was approved by the Human Investigation Committee of the Verona City Hospital. Metabolic tests  
480 were carried out on two separate days in random order<sup>48</sup>. Plasma glucose concentration was  
481 measured in duplicate with a Beckman Glucose Analyzer II (Beckman Instruments, Fullerton, CA,  
482 USA) or an YSI 2300 Stat Plus Glucose &Lactate Analyzer (YSI Inc., Yellow Springs, OH, USA)  
483 at bedside. Serum C-peptide and insulin concentrations were measured by chemiluminescence as  
484 previously described<sup>48</sup>. The analysis of the glucose and C-peptide curves during the OGTT was  
485 carried out with a mathematical model as described previously<sup>48</sup>. This model was implemented in  
486 the SAAM 1.2 software (SAAM Institute, Seattle, WA) to estimate its unknown parameters.  
487 Numerical values of the unknown parameters were estimated by using nonlinear least squares.  
488 Weights were chosen optimally, i.e., equal to the inverse of the variance of the measurement errors,  
489 which were assumed to be additive, uncorrelated, with zero mean, and a coefficient of variation  
490 (CV) of 6-8%. A good fit of the model to data was obtained in all cases and unknown parameters  
491 were estimated with good precision. In this paper we report the response of the beta cell to glucose  
492 concentration (proportional control of beta cell function), which in these patients accounts for  
493  $93.2 \pm 0.3\%$  of the insulin secreted by the beta cell in response to the oral glucose load. Genotypes  
494 were assessed by the high-throughput genotyping Veracode technique (Illumina Inc, CA), applying  
495 the GoldenGate Genotyping Assay according to manufacturer's instructions. Hardy-Weinberg  
496 equilibrium was tested by chi-square test. Variant association analyses were carried out by

497 generalized linear models (GLM) as implemented in SPSS 25.0 and they were adjusted for a  
498 number of potential confounders, including age, sex and BMI.

499 **iPSC generation, differentiation and genome editing (Fig. 4 and Supplementary Fig. 4 and 5)**

500 **iPSC generation and maintenance:** The human induced pluripotent stem cell line (hiPSC) SB  
501 Ad3.1 was previously generated and obtained through the IMI/EU sponsored StemBANCC  
502 consortium via the Human Biomaterials Resource Centre, University of Birmingham  
503 (<http://www.birmingham.ac.uk/facilities/hbrc>). Human skin fibroblasts were obtained from a  
504 commercial source (Lonza CC-2511, tissue acquisition number 23447). They had been collected  
505 from a Caucasian donor with no reported diabetes with fully informed consent and with ethical  
506 approval from the National Research Ethics Service South Central Hampshire research ethics  
507 committee (REC 13/SC/0179). The fibroblasts were reprogrammed to pluripotency as previously  
508 described<sup>49</sup> and were subjected to the following quality control checks: SNP-array testing via  
509 Human CytoSNP-12v2.1 beadchip (Illumina #WG-320-2101), DAPI-stained metaphase counting  
510 and mFISH, flow cytometry for pluripotency markers (BD Biosciences #560589 and 560126), and  
511 mycoplasma testing (Lonza #LT07-118).

512 **CRISPR-Cas9 mediated generation of p.Arg138\* and p.Lys34Serfs50\* human induced**  
513 **pluripotent stem cell line:** Several guide RNAs (gRNAs) were designed using MIT CRISPR tool  
514 (<http://crispr.mit.edu/>) to target near exon 2 and exon 3 of *SLC30A8* (ENST00000456015). The  
515 gRNAs were also subjected to an additional BlastN search ([www.ensembl.org](http://www.ensembl.org)) to confirm  
516 specificity and identified no additional off-target sites. To generate *SLC30A8*-p.Arg138\*, the target  
517 site for CRISPR-Cas9 mutagenesis (AGCAGGTACGGTTCATAGAG) was sub-cloned into the  
518 *BsbI* restriction sites within the gRNA structure in the pX330<sup>50</sup> plasmid that was previously  
519 modified to contain a puromycin selection cassette. A single strand oligonucleotide repair template  
520 for homology-directed repair (HDR) was synthesized by Eurogentec, stabilized by addition of a  
521 phosphorothioate linkage at the 5' end, and contained two nucleotide changes: i) the T2D-protective

nonsense mutation at codon-138 (c.412C>T, p.Arg138\*), which also mutated the PAM sequence, and ii) a silent mutation at codon-139 (c.417A>T, p.Ala139Ala) to introduce an *AluI* restriction site for genotyping. Human iPSCs were co-transfected with the *SLC30A8*-px330-puromycin resistant vectors and the HDR repair template using Fugene6 according to manufacturer's guidelines (Promega #E2691). Following transient puromycin-selection, single clones were picked and expanded as described previously<sup>51</sup>. Genotyping PCR was performed using primers (Forward: TACCCAGGAATGGCTTCTC; Reverse: ACGTGTTCTGTTGTCCCA) to amplify targeted region followed by *AluI* restriction digest. Successfully targeted clones were confirmed via Sanger sequence and monoallelic sequencing was performed by TA-cloning (pGEM®-T Easy Vector System; Promega #A1360) of the PCR amplicons. From 96 clones, 11 clones were heterozygous for p.Arg138\*, four of which contained indels in the non-targeted allele. The CRISPR-Sham hiPSC control line (p.Arg138Arg) was generated from hiPSC cells that went through the CRISPR pipeline without being edited at the *SLC30A8* locus. The two p.Arg138\* clones (A3 and B1) and the unedited control line (p.Arg138Arg) passed quality control checks that included repeat chromosome counting and pluripotency testing. Both p.Arg138\* clones were heterozygous for the c.412C>T, p.Arg138\*) while the silent variant at codon-139 (c.417A>T, p.Ala139Ala) was present in both alleles.

To generate *SLC30A8*-p.Lys34Serfs50\* the gRNA addressing the target site for CRISPR/Cas9 mutagenesis (GTGAATAAAGATCAGTGTCC) was synthesized using the Engen sgRNA synthesis kit (NEB) according to manufacturer's instruction. 20 uM of synthesized gRNA was reconstituted with 20 uM of Cas9 protein (NEB) and incubated at room temperature for 15 minutes to form a ribonucleoprotein (RNP) preparation of CRISPR/Cas9. A single strand oligonucleotide repair template for HDR containing the required seven nucleotide deletions (c.101\_107del, p.Lys34Serfs50\*) was synthesized (Eurogentec). Human iPSCs (1x10<sup>5</sup> cells) were electroporated with the RNP preparation and 50 uM of the repair template with the Neon Transfection

System from ThermoFisher Scientific using 10 uL tips (1200 volts, 30 ms, 2 pulses) according to manufacturer's guidelines. Following electroporation and single cell plating, single clones were picked and expanded as described previously. Genotyping PCR was performed using primers (Forward: TGGTGGCATTGACTGAATAAGA, Reverse: ACCCTCCCATAATGATGCAGA, and HDR-specific: GAAACCGGTGAATAGTGTCCCA) to amplify the target regions within exon 2 (511/504 bp) and the HDR-repaired allele (244 bp). Successfully targeted clones were confirmed via Sanger sequencing and monoallelic sequencing and passed quality control checks. From 96 clones, 11 clones were heterozygous for p.Lys34Serfs50\* but also contained indels in the other allele. Another 11 clones were homozygous for the variant, of which two were selected (clone B3 and D3).

***In vitro differentiation of hiPSCs towards Beta-like cells:*** Directed differentiation of hiPSCs towards beta-like cells was performed using a previously published protocol<sup>12,52</sup>. hiPSCs were seeded on Growth Factor Reduced Matrigel-coated CellBind 12-well tissue culture plates (Corning #356230 & #3336) at a cell density of  $1.3 \times 10^6$  in mTesR1 (Stem Cell Technologies #05850) with 10  $\mu$ M Y-27632 dihydrochloride (Abcam #ab120129). The following morning, hiPSCs were fed mTesR1 media >4 hours before starting the seven-stage differentiation protocol.

***Stage 1 (Definitive Endoderm):*** Cells were washed once with PBS before adding 0.5% bovine serum albumin (BSA; Roche #10775835001) MCDB131 media [(ThermoFisher Scientific #10372019) containing 1x Penicillin-Streptomycin (Sigma #P0781), 1.5 g/L sodium bicarbonate (ThermoFisher Scientific #25080060), 1x GlutaMAX™ (ThermoFisher Scientific #35050038) and 10 mM Glucose (ThermoFisher Scientific #A2494001)] supplemented with 100 ng/mL Activin A (Peprotech #120-14) and 3  $\mu$ M CHIR 99021 (Axon Medchem #1386). On day 2 and 3, cells were cultured with 0.5% BSA MCDB131 media supplemented with either 100 ng/mL Activin A and 0.3  $\mu$ M CHIR 99021 (day 2) or with 100 ng/mL Activin A alone (day 3).

***Stage 2 (Primitive Gut Tube):*** Cells were cultured for 48 hours in 0.5% BSA MCDB131 media with 0.25 mM ascorbic acid (Sigma #A4544) and 50 ng/mL KGF (PeproTech #100-19).

572 Stage 3 (Posterior Foregut): Cells were cultured for two days in 2% BSA MCDB131 media  
573 supplemented with 1 g/L sodium bicarbonate, 0.25 mM ascorbic acid, 0.5x Insulin-Transferrin-  
574 Selenium-Ethanolamine (ITS-X; ThermoFisher Scientific #51500056), 1  $\mu$ M retinoic acid (RA;  
575 Sigma-Aldrich #R2625), 0.25  $\mu$ M Sant-1 (Sigma-Aldrich #S4572), 50 ng/ml KGF, 100 nM  
576 LDN193189 (Stemgent #04-0074), and 100 nM  $\alpha$ -Amyloid Precursor Protein Modulator (Merck  
577 #565740).

578 Stage 4 (Pancreatic Endoderm): Cells were cultured for three days in 2% BSA MCDB131 media  
579 supplemented with 1 g/L sodium bicarbonate, 0.25 mM ascorbic acid, 0.5x ITS-X, 0.1  $\mu$ M RA, 0.25  
580  $\mu$ M Sant-1, 2 ng/ml KGF, 200 nM LDN193189 and 100 nM  $\alpha$ -Amyloid Precursor Protein  
581 Modulator.

582 Stage 5 (Endocrine Progenitors): Cells remained in planar culture for three days in 2% BSA  
583 MCDB131 media supplemented with 20 mM final glucose, 0.5x ITS-X, 0.05  $\mu$ M RA, 0.25  $\mu$ M  
584 Sant-1, 100 nM LDN193189, 10  $\mu$ M ALK5 Inhibitor II (Enzo Life Sciences #ALX-270-445), 1  $\mu$ M  
585 3,3,5-Triiodo-L-thyronine sodium salt (T3; Sigma-Aldrich #T6397), 10  $\mu$ M zinc sulfate  
586 heptahydrate (Sigma # Z0251), and 10  $\mu$ g/mL heparin sodium salt (Sigma #H3149).

587 Stage 6 (Endocrine Cells): Cells remained in planar culture for six days in 2% BSA MCDB131  
588 media supplemented with 20 mM final glucose, 0.5x ITS-X, 100 nM LDN193189, 10  $\mu$ M ALK5  
589 Inhibitor II, 1  $\mu$ M T3, 10  $\mu$ M zinc sulfate heptahydrate, and 100 nM  $\gamma$ -Secretase Inhibitor XX  
590 (Merck Millipore #565789).

591 Stage 7 (Beta-like Cells): Cells remained in planar culture for another six days in 2% BSA  
592 MCDB131 media supplemented with 20 mM final glucose, 0.5x ITS-X, 10  $\mu$ M ALK5 Inhibitor II,  
593 1  $\mu$ M T3, 1 mM N-Cys (Sigma-Aldrich #A9165), 10  $\mu$ M Trolox (EMD Millipore #648471), 2  $\mu$ M  
594 R248 (SelleckChem #S2841), and 10  $\mu$ M zinc sulfate heptahydrate.



595 ***Quantification of SLC30A8 gene expression in Beta-like Cells derived from CRISPR-edited***  
596 ***hiPSCs:*** Expression of *SLC30A8* was measured at the end of stage 7 using quantitative PCR  
597 (qPCR). Briefly, RNA was extracted using TRIzol Reagent (Life Technologies #15596026)  
598 according to manufacturer's instructions. cDNA was amplified using the GoScript Reverse  
599 Transcription Kit (Promega #A5000). qPCR was performed using 40 ng of cDNA, TaqMan® Gene  
600 Expression Master Mix (Applied Biosystems #4369017) and primer/probes for *SLC30A8*  
601 (Hs00545182\_m1) or the housekeeping gene *TBP* (Hs00427620\_m1). Gene expression was  
602 determined using the  $\Delta\Delta CT$  method by first normalizing to *TBP* and then to the control  
603 p.Arg138Arg (n=7-13 wells from three differentiations).

604 ***Allele-specific SLC30A8 expression in beta-like Cells derived from CRISPR-edited hiPSCs:***  
605 Stage 7 cells were treated with 100  $\mu$ g/mL cycloheximide (Sigma #C4859) or DMSO (Sigma  
606 #D2650) for four hours at 37°C<sup>53</sup> before or RNA and cDNA synthesis as above. Allele specific  
607 expression was measured using the QX10 Droplet Digital PCR System and C1000 Touch Thermal  
608 Cycler according to manufacturer's guidelines (Bio-Rad). Custom primers and probes for the  
609 detection of p.Arg138\* variant were designed using Primer3Plus (Applied Biosystems): Forward  
610 primer AGTCTCTTCTCCCTGTGGTT; Reverse primer ATGATCATCACAGTCGCCTG; FAM  
611 probe (R138; CT) 5'-FAM-ATGGCACCGAGCTGA-MGB-3'; VIC probe (X138; TT) 5'-VIC-  
612 ATGGCACCTGAGCTGAGA-MGB-3'. The specificity of the probes was confirmed by ddPCR  
613 using R138 or X138 templates (Supplementary Fig. 5). Results were analysed using Quanta Soft  
614 software (Bio-Rad) and presented as a ratio of wildtype to HDR-edited allele expression (n>4 wells  
615 from two differentiations).

616 ***Allele-specific SLC30A8 expression by targeted RNA sequencing of SLC30A8 (Figure 4e and***  
617 ***Supplementary Fig. 5c):*** Dual-indexed RNA libraries were prepared with target specific priming of  
618 both strand synthesis from 50 ng of extracted RNA from p.Arg138\* edited (clone A3 and B1) and  
619 unedited Beta-like Cells derived from hiPSC using QuantSeq-Flex Targeted RNA-Seq Library Prep

620 Kit V2 (Lexogen GmbH, Vienna, Austria) according to user guide version 015UG058V0230.  
621 Targeted primers covering p.Arg138\* mutation, 5- AGTCTCTTCTCCCTGTGGTT -3'  
622 and 5- ATGATCATCACAGTCGCCTG -3', were generated and further modified with partial  
623 Illumina P7 and P5 adapter extensions. For normalization of the data, 6 base pair unique molecular  
624 identifier (UMI) was included into first strand synthesis primer. Quality of libraries was measured  
625 using 2100 Bioanalyzer DNA High Sensitivity Kit (Agilent, Santa Clara, CA, USA). Linker-linker  
626 artifacts were removed with BluePippin DNA size-selection (Sage Science Inc., Beverly, MA,  
627 USA) before pooling the libraries to the sequencing run. Sequencing (2x250 bp) was performed  
628 with Illumina MiSeq system using v2 chemistry (Illumina, San Diego, CA, USA). Target RNA  
629 sequencing reads were aligned to hg38 using STAR (Spliced Transcripts Alignment to Reference)<sup>54</sup>,  
630 <sup>55</sup> and UMI-tools<sup>56</sup> used to remove PCR based duplications (deduplication) using 6 bp UMI in read  
631 2.

632 *SLC30A8 and INS transcript expression in hiPSC-derived BLCs by RNAscope® (Supplementary*  
633 *Fig. 5e-g):* Stage 7 cells were trypsinized and the resulting single cell suspension was subjected to  
634 cytopsin (~50,000 cells/slot) for 5 minutes at 1200 rpm. Samples were then fixed in 10% neutral  
635 buffered formalin for 40 minutes at 37°C, washed once in PBS and slides were dehydrated for 5  
636 minutes at room temperature in 50%, 70%, and 2x5 minutes in 100% ethanol before storage at -  
637 20°C. Before proceeding with the RNAScope® In Situ Hybridization Technology (Advanced Cell  
638 Diagnostics, Inc.), samples were rehydrated and processed following the manufacturer's  
639 recommendations for cultured adherent cell sample preparation using the RNAscope® Multiplex  
640 Fluorescent Reagent Kit\_v2 (ACDbio#323100). For hybridization, RNAscope® Probe-Hs-  
641 *SLC30A8* (ACDbio#441261) and RNAscope® Probe-Hs-*INS*-C2 (ACDbio#313571-C2) were used.  
642 For detection, Cy3 fluorophore (PerkinElmer TSA Plus Cyanine 3 System #NEL744E001KT) was  
643 used to detect *SLC30A8* and Cy5 (PerkinElmer TSA Plus Cyanine 5 System #NEL745E001KT)  
644 was used to detect *INS* at 1:1500 dilution. Samples were counterstained with DAPI to detect nuclei

645 and mounted with ProLong Gold Antifade Mountant (Thermofisher). A minimum of six  
646 independent fields were captured using a Nikon Eclipse TE2000-U Epifluorescence microscope  
647 with a plan fluor ELWD 20x ADL objective. Independent images were analyzed using QuPath  
648 v0.1.2 and the cell mean intensity for each was measured. Once background was subtracted, cells  
649 with values of *SLC30A8* > 10 were included.

650 **Western blot of ZnT8:** We used highly specific antibody for ZnT8 as developed by Merriman et  
651 al<sup>57</sup>. Cell pellets were lysed in RIPA buffer (50mM Tris pH 7.4, 150mM NaCl, 1% Triton X-100,  
652 0.5% sodium deoxycholate, 0.1% SDS) containing 1x protease inhibitor cocktail (Roche). Protein  
653 samples were prepared in Laemmli buffer and not heat denatured. 10µg of protein were loaded on a  
654 Mini-PROTEAN TGX 4-20% precast gel (Bio-Rad) and run at 300V for 15minutes. The gel was  
655 activated on a ChemiDoc MP Imaging System and transferred to a Trans-Blot Turbo polyvinylidene  
656 fluoride (PVDF) membrane using the Trans-Blot Turbo Transfer System (all Bio-Rad). Membranes  
657 were blocked in 5% milk for 1h at RT, incubated with primary antibody against Znt8 ((1), 1:1000)  
658 overnight at 4°C followed by 1h incubation at RT with HRP-coupled secondary anti-mouse IgG  
659 antibody (Thermo Scientific 31450, 1:2500). The membranes were subsequently incubated for 4  
660 min. at RT with Clarity Western enhanced chemiluminescence (ECL) reagent and imaged on the  
661 ChemiDoc MP Imaging System (Bio-Rad). Western Blot images were quantified using Image Lab  
662 software (Bio-Rad) and normalised to a loading control on the same blot ( $\beta$ -tubulin (Santa Cruz, sc-  
663 365791, 1:2000).

#### 664 **EndoC- $\beta$ H1 culture (Fig. 5)**

665 The results obtained in EndoC- $\beta$ H1 are from two distinct teams (Helsinki and Oxford) with  
666 different batches of EndoC- $\beta$ H1 cultures. Here, we report both methods and specify for each  
667 experiment the origin of the culture (Helsinki or Oxford). EndoC- $\beta$ H1 cells were cultured in  
668 medium and grown on a matrix as described previously<sup>58</sup> and tested negative for mycoplasma.

***SLC30A8 knockdown in EndoC-βH1 cells:*** In Oxford, EndoC-βH1 cells were transfected with 10 nM siRNA (either SMARTpool ON-TARGETplus SLC30A8 or scramble [Dharmacon #L-007529-01]) and Lipofectamine RNAiMAX (Life Technologies #13778-075) according to manufacturer's instructions for a total of 72 hours. In Helsinki, EndoC-βH1 cells were transfected using Lipofectamin RNAiMAX (life technologies). 20nM siRNA ON-TARGET*plus* siRNA SMARTpool for human *SLC30A8* gene (Dharmacon; L-007529-01) and ON-TARGET*plus* Non-targeting pool (siNT or Scramble) (Dharmacon; D-001810-10-05) were used following the protocol as described previously<sup>59</sup>. Cells were harvested 96 h post-transfection for further studies.

***Insulin secretion measurements in EndoC-βH1 cells:*** In Oxford, cells were subjected to static insulin secretion assays 72hrs after siRNA transfection as described previously<sup>59</sup>, apart from the following modifications: cells were stimulated for 1 hr with 1 mM glucose, 20 mM glucose, 1 mM glucose + 200 μM tolbutamide, or 20 mM glucose + 500 μM diazoxide. Insulin levels were measured in both supernatants and cells using the Insulin (human) AlphaLISA Detection Kit and EnSpire Alpha Plate Reader (Perkin Elmer #AL204C and #2390-0000, respectively). Cell count per well was measured via CyQUANT Direct Cell Proliferation Assay (Thermo Fisher# C35011). Data are presented as insulin secretion normalized to percentage of insulin content from Control condition. RNA extraction, cDNA synthesis, and qRT-PCR was performed as above (*SLC30A8* gene expression in CRISPR-edited hiPSCs derived beta like cell section) to determine *SLC30A8* knockdown and expression of the K<sub>ATP</sub> channel genes (*ABCC8* Hs01093752\_m1 and *KCNJ11* Hs00265026\_s1; ThermoFisher Scientific). In Helsinki, EndoC-βH1 cells were transfected with 20nM siRNA and Scramble control<sup>60</sup>. Following 96h of siRNA transfection, cells were incubated overnight in 1 mM glucose containing EndoC-βH1 culture medium. One hour prior to glucose stimulation assay, the media was replaced by βKREBS (Univercell Biosolution S.A.S., France) without glucose. Cells were stimulated with 16.7 mM glucose and 50 mM KCl (Sigma-Aldrich) in βKREBS for 30 minutes at 37°C in a CO<sub>2</sub> incubator. The cells were then washed and lysed with

694 TETG (Tris pH8, Trito X-100, Glycerol, NaCl and EGTA) solution (Univercell Biosolution S.A.S.,  
695 France) for the measurement of total insulin content. Secreted and intracellular insulin were  
696 measured using a commercial human insulin Elisa kit (Mercodia AB, Uppsala, Sweden) as per  
697 manufacturer's instructions (Helsinki).

698 ***Electrophysiological measurements in EndoC-βH1 cells (Oxford):*** *SLC30A8* was knocked down  
699 in EndoC-βH1 as above.  $K^+_{ATP}$  channel conductance was measured in a perforated patch whole cell  
700 configuration, and patch-clamped using an EPC 10 amplifier and HEKA pulse software. KREBS  
701 extracellular solution was perfused in at 32°C and contained: 138 mM NaCl, 3.6 mM KCl, 0.5 mM  
702  $MgSO_4$ , 10 mM HEPES, 0.5 mM  $NaH_2PO_4$ , 5 mM  $NaHCO_3$ , 1.5 mM  $CaCl_2$ , 1 mM glucose and 100  
703  $\mu M$  Diazoxide (Sigma-Aldrich #D9035). The perforation of the membrane was achieved using an  
704 intra-pipette solution containing: 0.24 mg/mL amphotericin B, 128 mM K-gluconate (Sigma  
705 #Y0000005 and G4500 respectively), 10 mM KCl, 10 mM NaCl, 1 mM  $MgCl_2$ , 10 mM HEPES,  
706 pH 7.35 (KOH). Conductance data are normalized to cell size and presented as pS.pF<sup>-1</sup>. Expression  
707 of *ABCC8*, *KCNJ11*, *B2M*, and *TBP* were measured via qPCR as above (*SLC30A8* gene expression  
708 in CRISPR-edited hiPSCs derived beta like cell section).

709 ***Insulin and proinsulin secretion and content (Helsinki):*** For the measurement of secreted insulin  
710 or proinsulin in the supernatant, 96h post-transfected cells were washed twice with 1X PBS and  
711 incubated with fresh EndoC-βH1 culture medium for next 24h. Secreted and intracellular insulin  
712 and proinsulin were measured using a commercial human insulin Elisa and human proinsulin Elisa  
713 kit from Mercodia (Mercodia AB, Uppsala, Sweden). Proinsulin to insulin ratio was calculated by  
714 dividing the respective values measured from the supernatant and the cells (pmol/L).

715 ***Immunoblotting (Helsinki and Oxford):*** Total cellular protein was prepared with Laemmli buffer  
716 and resolved using Any kD Mini-Protean-TGX gel (Bio-Rad). Immunoblot analysis was performed  
717 by overnight incubation of with primary antibodies against PC1/3 (Cell Signaling; #11914; 1:1000),  
718 CPE (BD Bioscience; #610758; 1:1000), PC2 (Santa-Cruz; #SC-374140; 1:450), Phospho-AKT-

719 Ser473 (Cell Signaling; #4060; 1:1000) and AKT (Santa-Cruz; #SC-8312; 1:500). The membranes  
 720 were further incubated with species-specific HRP-linked secondary antibodies (1:5000) and  
 721 visualization was performed following ECL exposure with ChemiDoc XRS+ system and Image Lab  
 722 Software (Bio-Rad). A loading control of either alpha-Tubulin (Sigma; T5168; 1:5000) or beta-  
 723 actin (Sigma; A5441; 1:5000) was performed on the same blot for all western blot data.  
 724 Densitometric analysis of bands from image were calculated using Image J (Media Cybernetics)  
 725 software and intensities compared as PC1/3, phosphor-AKT-Ser473, PC2 to tubulin; CPE to beta-  
 726 actin. [Western blot for ZnT8 was performed as described previously in iPSC section.](#)

727 ***Cell viability assay, MTT (Helsinki):*** EndoC-βH1 cells were transfected with either siScramble or  
 728 siSLC30A8 for 96h. The viability of cells after 24 h of tunicamycin (10 µg/ml) treatment was  
 729 determined using Vybrant MTT Cell proliferation kit (ThermoFisher Scientific; #M6494), the  
 730 standard MTT [3-(4,5-dimethylthiazol-2-yl)-2,5-diphenyltetrazolium bromide] assay. All the  
 731 treatments were performed on cells with equal seeding density (5×10<sup>4</sup> cells/well) in 96 wells plate.  
 732 The purple formazan crystals generated after 2 h incubation with MTT buffer were dissolved in  
 733 DMSO, and the absorbance was recorded on a microplate reader at a wavelength of 540nm.

734 [\*\*\*Zinpyr-1 based Zinc staining in EndoC-βH1 cells \(Helsinki\):\*\*\*](#) EndoC-βH1 cells, 1.5 x 10<sup>5</sup> cells per  
 735 well of 24-well plate (Costar #3526) were treated with siRNA against *SLC30A8* or Non-targeted  
 736 control as described previously in siRNA methods section. After 96 h siRNA treatment, cells were  
 737 washed twice with KRBH complete buffer containing 5.5mM glucose and load with zinc-specific  
 738 fluorescent dye Zinpyr-1 (5µM, Cayman Chemicals #15122) for 30 minutes in the cell culture  
 739 incubator<sup>61</sup>. Then, fluorescent images were obtained after rinsed in KRBH buffer, with an IncuCyte-  
 740 S3 Live-Cell Imaging system (Essen BioScience) using 488 nm laser. Images were analyzed with  
 741 IncuCyte S3 software and presented as ratio of green mean intensity object average to phase area  
 742 confluency.

743 *Assessment of granule zinc content: monitoring of stimulated zinc secretion using ZIMIR*  
744 *(Supplementary Fig. 6):*

745 EndoC- $\beta$ H1 cells were seeded on glass slides and transfected with siRNA control or targeted  
746 against *SLC30A8* (SMARTpool ON-targetplus) at a final concentration of 20nM using  
747 Lipofectamine RNAiMax (Thermo Fisher) according to manufacturer's instruction. 72 h post-  
748 transfection, cells were incubated for 2 h in culture media containing 3mM glucose and then for 20  
749 minutes in KHB buffer saturated with 95% O<sub>2</sub>/5% CO<sub>2</sub> and adjusted to pH 7.4, containing 3 mM  
750 glucose and 5 $\mu$ M Zinc binding probe zinc indicator for monitoring induced exocytotic release  
751 (ZIMIR<sup>15</sup>). Cells were then transferred to an imaging chamber and acquisitions were performed in  
752 KHB buffer with KCl added (20mM final concentration) 3 minutes after acquisition began.

753 Total internal reflection of fluorescence (TIRF) imaging was performed on a Nikon Eclipse Ti  
754 microscope equipped with a 100x/1.49NA TIRF objective, a TIRF/FRAP iLas2 module to control  
755 laser angle (Roper Scientific), a Quad Band TIRF Filter Cube (TRF89902 – Chroma) and an ibidi  
756 heating system. ZIMIR was excited using a 488 nm laser line, and images were acquired with an  
757 ORCA-Flash 4.0 camera (Hamamatsu). Metamorph software (Molecular Devices) was used for  
758 data capture. Image analysis was performed using ImageJ, to measure fluorescence intensity close  
759 to (within ~70 nm of) the plasma membrane. Traces are presented as normalized intensity over time  
760 (F/F<sub>0</sub>).

761 ***RNA (mRNAs) sequencing of EndoC- $\beta$ H1 cells (Supplementary Fig. 7):*** For RNA sequencing  
762 post 96h siScramble (n=8) or siSLC30A8 (n=8) transfected EndoC- $\beta$ H1 cells were used and the  
763 total RNA was extracted with Macherey-Nagel RNA isolation kit as per manufacturer's instruction.  
764 RNA sequencing was performed using Illumina TruSeq-mRNA library on NextSeq 500 system  
765 (Illumina) with an average of >15 million paired-end reads (2  $\times$  75 base pairs). RNA sequencing  
766 reads were aligned to hg38 using STAR (Spliced Transcripts Alignment to Reference)<sup>54</sup>, genome  
767 annotations were obtained from the GENCODE (Encyclopedia of Genes and Gene Variants) v22<sup>55</sup>

768 program, and reads counting were done using featureCounts<sup>62</sup>. Further downstream analysis was  
769 perform using edgeR<sup>63</sup> software package, low expressed (<-1 median log 2 transformed counts per  
770 gene) genes were removed, read counts were normalized using TMM<sup>64</sup> (trimmed mean of M-  
771 values), differential expression analysis was performed using method similar to Fisher's Exact Test  
772 (as implemented in edgeR) and corrected for multiple testing using Bonferroni method. Over-  
773 representation analysis among differentially expressed genes against 12 different pathway data  
774 bases (Reactome, BioCarta, KEGG, Wikipathways, EHMN, HumanCyc, INOH, NetPath,  
775 PharmGKB, PID, Signalink, SMPDB), as implemented in ConsensusPathDB (Release 34)<sup>65</sup>, was  
776 performed using a hypergeometric test and corrected for multiple correction (FDR correction).  
777 The gene set enrichment analysis was performed using GSEA software (GSEA vs 3.0)<sup>66</sup> against  
778 gene ontology database (c5.all.v6.2.symbols.gmt) with 1000 permutations.

779 **Data Analyses:** Data are reported as mean (SEM). Statistical analyses were performed using Prism  
780 6.0 (GraphPad Software). All parameters were analyzed using Mann-Whitney test or one sample t  
781 test as indicated.

## 782 **Mouse Model (Fig. 6)**

783 **Animals:** All procedures were conducted in compliance with protocols approved by the Regeneron  
784 Pharmaceuticals Institutional Animal Care and Use Committee. The *Slc30a8*<sup>Tgp.Arg138\*</sup> mouse line is  
785 made in pure C57Bl/6 background by changing nucleotide 409 from T into C in exon 3, which  
786 changes the arginine into a stop codon<sup>10</sup>. The mutated allele has a self-deleting neomycin selection  
787 cassette flanked by loxP sites inserted at intron 3, deleting 29 bp of endogenous intron 3 sequence.  
788 Mice were housed (up to five mice per cage) in a controlled environment (12-h light/dark cycle,  
789 22C, 60–70% humidity) and fed *ad libitum* with either chow (Purina Laboratory 23 Rodent Diet  
790 5001, LabDiet) or high-fat diet (Research Diets, D12492; 60% fat by calories) starting at age of 10  
791 to 20 weeks. All data shown are compared to their respective WT littermates.



792 **Glucose Tolerance Test:** Mice were fasted overnight (16 hr) followed by oral gavage of glucose  
793 (Sigma) at 2 g/kg body weight. Blood samples were obtained from the tail vein at the indicated  
794 times and glucose levels were measured using the AlphaTrak2 glucometer (Abbott). Submandibular  
795 bleeds for insulin were done at 0, 15, and 30 minutes post-injection in a separate experiment to not  
796 interfere with glucose levels.

797 **Hormone measurements:** Submandibular bleeds of either overnight fasted (16 hrs) animals were  
798 done in the morning. Plasma insulin or proinsulin was analyzed with the mouse insulin/proinsulin  
799 EIA (Mercodia AB, Uppsala, Sweden), and C-peptide with the mouse C-peptide EIA (ALPCO). All  
800 EIAs were performed according to the manufacturer's instructions.

801 **Data Analyses for mouse studies:** Data are reported as mean (SEM). Statistical analyses were  
802 performed using Prism 8.0 (GraphPad Software). [All parameters were analyzed by two-way](#)  
803 [ANOVA combined with Sidak's multiple comparison test, or Mann Whitney test as indicated.](#)

804 **Expression of p.Arg138\* mutation in INS1E (Supplementary Fig. 8)**

805 INS-1E cells<sup>67</sup> were used for transient transfection of pcDNA3.1(+)-p.Arg138\* construct fused to  
806 fluorescent m-Cherry at C-terminus using transfection reagent Viromer according to the  
807 manufacturer's instructions. After transfections cells were collected at 24, 48, 72 and 96 hours and  
808 analyzed by western blot analysis using mCherry (600-401-P16, Rockland) antibody. Untransfected  
809 cells were used as control and tubulin as a loading control. Two days after transient transfections  
810 with either p.Arg138\*-mCherry (INS1E), p.Arg138\*-HA or p.Arg138\*-Myc-His construct  
811 (INS1E), cells were washed with PBS twice and fixed using 4% paraformaldehyde for 15 minutes  
812 at room temperature. Cells were permeabilized with 0.2 % Triton X-100 in phosphate-buffered  
813 saline (PBS) for 10 mins and to prevent unspecific binding were further blocked for 1 h with 5%  
814 FBS in PBS. INS1E cells transfected with either p.Arg138\*-HA or p.Arg138\*-Myc-His construct  
815 were incubated with the primary antibody (HA antibody: MMS-101P, Biolegend; His antibody:

816 D291-A48, MBL; insulin antibody: A0564, DAKO), overnight at 4°C. Secondary antibodies were  
817 conjugated to Alexa Fluor 488 (Molecular Probes). Cells transfected with mCherry construct were  
818 imaged after 48 and 96 hours (INS1E) in order to visualize subcellular localization at different time  
819 points.

820 **Measurements of cytosolic zinc in INS-1(832/13) cells ([Supplementary Fig. 8](#))**

821 **Cell culture:** INS-1 (823/13) cells were grown in RPMI 1640 medium (Sigma-Aldrich, UK)  
822 supplemented with 10% (v/v) foetal bovine serum (FBS), 2 Mm L-glutamine, 0.05 mM 2-  
823 mercaptoethanol, 10 mM HEPES (Sigma-Aldrich), 1 mM sodium pyruvate (GIBCO, France), 2  
824 mM L-glutamine and antibiotics (100 µg/ml Streptomycin and 100 U/ml penicillin). Cells were  
825 maintained in 95% oxygen, 5% carbon dioxide at 37°C.

826 **Co-transfection:** Cells were seeded on sterile coverslips at 60% confluence and co-transfected  
827 using lipofectamine 2000 (Invitrogen, USA) according to the manufacturer's instructions, with  
828 either the empty construct (EV) or the rare-truncated variant (c-Myc tag, R138X) construct and the  
829 Förster Resonance Energy transfer sensors (FRET), eCALWY-4 vector (free cytosolic zinc  
830 measurements).

831 **Protein extraction and Western (immuno-) blotting analysis:** For protein extraction, RIPA buffer  
832 (1% Triton X-100, 1% sodium deoxycholate, 0.1% SDS, 0.15 mM NaCl, 0.01 M sodium Phosphate  
833 pH7.2) was used for lysis. Protein extracts were resolved in SDS-page (12% vol/vol acrylamide)  
834 and transferred to a polyvinylidene fluoride (PVDF) membrane, followed by blocking for 1 hour,  
835 immunoblotting with either c-Myc anti-mouse SLC30A8 (1:400) and the secondary anti-mouse  
836 antibody (1:10000, Abcam), and then the mouse monoclonal anti-tubulin (1:10000) and secondary  
837 anti-mouse for tubulin (1:5000). Chemiluminescence detection reagent (GE Healthcare) was used  
838 before exposing to hyperfilms.

**Immunocytochemistry:** Cells were fixed in 4% (v/v) Phosphate-buffered saline/Paraformaldehyde (PFA). Cells were permeabilized in 0.5% (w/v) PBS/TritonX-100 and further saturated with PBS/BSA 0.1%. Cells were then incubated for 1 hour with the primary antibody, anti-c-Myc mouse antibody (1:200) followed by the secondary Alexa Fluor® 568 nm anti-mouse IgG (H+L, 1:1000 Life Technologies, USA). Coverslips were mounted with mounting medium containing DAPI (Vectashield, USA) on microscope slides (ThermoScientific). Imaging was performed on a Nikon Eclipse Ti microscope equipped with a 63x/1.4NA objective, spinning disk (CAIRN, UK) using a 405, 488 and 561 nm laser lines, and images were acquired with an ORCA-Flash 4.0 camera (Hamamatsu) Metamorph software (Molecular Device) was used for data capture.

**Cytosolic free  $Zn^{2+}$  measurements:** Cells were co-transfected with R138X (p.Arg138\*) construct or empty construct (EV) and eCALWY-4 construct. Acquisitions were performed 24 hours after transfection using an Olympus IX-70 wide-field microscope with a 40x/1.35NA oil immersion objective and a zyla sCMOS camera (Andor Technology, Belfast, UK) controlled by Micromanager software. Excitation was provided at 433 nm using a monochromator (Polychrome IV, Till Photonics, Munich, Germany). Emitted light was split and filtered with a Dual-View beam splitter (Photometrics, Tucson, Az, USA) equipped with a 505dexc dichroic mirror and two emission filters (Chroma Technology, Bellows Falls, VT, USA - D470/24 for cerulean and D535/30 for citrine). Cells were perfused for 4 minutes with KREBS buffer (140 mM NaCl, 3.6 mM KCl, 0.5 mM  $NaH_2PO_4$ , 0.2 mM  $MgSO_4$ , 1.5 mM  $CaCl_2$ , 10 mM HEPES, 25 mM  $NaHCO_3$ ) without additives, next the buffer was changed to KREBS buffer containing 50  $\mu M$  N,N,N',N'-tetrakis(2-pyridylmethyl)ethylenediamine (TPEN, Sigma) for 5 minutes, followed by perfusion with KREBS buffer containing 100  $\mu M$   $ZnCl_2$  and 5  $\mu M$  of the  $Zn^{2+}$ -specific ionophore 2-mercaptopyridine N-oxide (Pyrithione, Sigma). Image analysis was performed using ImageJ software. Steady-state fluorescence intensity ratio of acceptor over donor was measured, followed by the determination of the minimum and maximum ratios to calculate the free  $Zn^{2+}$  concentration using the following

864 formula:  $[Zn^{2+}] = K_d \cdot ( (R - R_{min}) / (R_{max} - R) )$ , in which  $R_{min}$  is the ratio in the  $Zn^{2+}$  depleted  
865 state, after addition of 50  $\mu M$  TPEN, and  $R_{max}$  was obtained upon  $Zn^{2+}$  saturation with 100  $\mu M$   
866  $ZnCl_2$  in the presence of 5  $\mu M$  pyridithione.

#### 867 **Human Pancreatic Islets (Fig. 7)**

868 Experiments on primary human pancreatic islets were independently performed in two places 1)  
869 Oxford and 2) Lund university diabetes center (LUDC)

870 ***Human pancreatic islets from Oxford:*** Human pancreatic islets were isolated from deceased  
871 donors under ethical approval obtained from the human research ethics committees in Oxford  
872 (REC: 09/H0605/2, NRES committee South Central-Oxford B). All donors gave informed research  
873 consent as part of the national organ donation program. Islets were obtained from the Diabetes  
874 Research & Wellness Foundation Human Islet Isolation Facility, OCDEM, University of Oxford.  
875 All methods and protocols using human pancreatic islets were performed in accordance with the  
876 relevant guidelines and regulations in the UK (Human Tissue Authority, HTA). For *in vitro* insulin  
877 secretion, islets were pre-incubated in Krebs-Ringer buffer (KRB) containing 2 mg/mL BSA and  
878 1 mM glucose for 1 hour at 37°C, followed by 1-hour stimulation in KRB supplemented with 6mM  
879 glucose. Insulin content of the supernatant was determined by radioimmunoassay (Millipore UK  
880 Ltd, Livingstone, UK) as described previously<sup>68</sup>.

881 ***Human pancreatic islets from LUDC:*** Human pancreatic islets were obtained from the Human  
882 Tissue Laboratory (Lund University, [www.exodiab.se/home](http://www.exodiab.se/home)) in collaboration with The Nordic  
883 Network for Clinical Islet Transplantation Program ([www.nordicislets.org](http://www.nordicislets.org))<sup>69,70</sup>. All the islet donors  
884 provided their consent for donation of organs for medical research and the procedures were  
885 approved by the ethics committee at Lund University (Malmö, Sweden, permit number 2011263).  
886 Islet preparation for cadaver donors, their purity check and counting procedure have been described  
887 previously<sup>71</sup>. Static *in vitro* insulin secretion assay from 91 islets (non-diabetic individuals) was

performed as described previously<sup>71,72</sup>. Briefly, six batches of 12 islets per donor were incubated for 1 hour at 37°C in Krebs Ringer bicarbonate (KRB) buffer in presence of 1 mM or 16.7 mM glucose. Independently, KCL based insulin secretion assay was performed by incubating them in 70 mM KCl together with 1 mM or 16.7 mM glucose in a subset of islets in different batches. Insulin concentrations in the extracts were measured using a radioimmunoassay kit (Euro-Diagnostica, Malmö, Sweden). The Association of p.Trp325Arg genotype with expression of *SLC30A8* and other candidate genes was performed using RNA sequencing from islets of 139 non-diabetic individuals as described previously<sup>69,70</sup>. Briefly, RNA sequencing of islets was done using a HiSeq 2000 system (Illumina) for an average depth of 32.4 million paired-end reads (2 × 100 base pairs)<sup>69,70</sup>. RNA sequencing reads were aligned to hg19 using STAR (Spliced Transcripts Alignment to Reference)<sup>54</sup>. Genome annotations were obtained from the GENCODE (Encyclopedia of Genes and Gene Variants) v20<sup>55</sup> program and read counting was done using featureCounts<sup>62</sup>. Read counts were normalized to total reads (counts per million) and additionally across-samples normalization was done using TMM method<sup>64</sup>. Association analysis (so called eQTL) was performed on inverse normalized expression values using linear regression adjusted for age, sex and islets purity using PLINK<sup>36</sup>.

**Statistics**

Detail information regarding statistical tests used for each sub-study has been provided in their respective method section or with figure legends.

**Data Availability**

The data that support the findings of this study are available from the corresponding author on reasonable request. Individual level data for the human study can only be obtained via the Biobank of The Institute of Health and Welfare in Finland. [The raw count data for RNA sequencing are available in Supplementary Data Set 1.](#)

## 912    **References**

- 913        1. Chabosseau, P. & Rutter, G. A. Zinc and diabetes. *Arch. Biochem. Biophys.* **611**, 79-85 (2016).
- 914        2. Chimienti, F., Devergnas, S., Favier, A. & Seve, M. Identification and cloning of a beta-cell-specific zinc
- 915        transporter, ZnT-8, localized into insulin secretory granules. *Diabetes* **53**, 2330-7 (2004).
- 916        3. Flannick, J. et al. Loss-of-function mutations in SLC30A8 protect against type 2 diabetes. *Nat. Genet.* **46**,
- 917        357-63 (2014).
- 918        4. Parsons, D. S., Hogstrand, C. & Maret, W. The C-terminal cytosolic domain of the human zinc transporter
- 919        ZnT8 and its diabetes risk variant. *FEBS J.* **285**, 1237-1250 (2018).
- 920        5. Sladek, R. et al. A genome-wide association study identifies novel risk loci for type 2 diabetes. *Nature* **445**,
- 921        881-5 (2007).
- 922        6. Lemaire, K. et al. Insulin crystallization depends on zinc transporter ZnT8 expression, but is not required for
- 923        normal glucose homeostasis in mice. *Proc. Natl. Acad. Sci. U S A* **106**, 14872-7 (2009).
- 924        7. Pound, L. D. et al. Deletion of the mouse Slc30a8 gene encoding zinc transporter-8 results in impaired
- 925        insulin secretion. *Biochem. J.* **421**, 371-6 (2009).
- 926        8. Wijesekara, N. et al. Beta cell-specific Znt8 deletion in mice causes marked defects in insulin processing,
- 927        crystallisation and secretion. *Diabetologia* **53**, 1656-68 (2010).
- 928        9. Mitchell, R. K. et al. Molecular Genetic Regulation of Slc30a8/ZnT8 Reveals a Positive Association with
- 929        Glucose Tolerance. *Mol. Endocrinol.* **30**, 77-91 (2016).
- 930        10. Kleiner, S. et al. Mice harboring the human SLC30A8 R138X loss-of-function mutation have increased
- 931        insulin secretory capacity. *Proc. Natl. Acad. Sci.* **115**, E7642-E7649 (2018).
- 932        11. Groop, L. et al. Metabolic consequences of a family history of NIDDM (the Botnia study): evidence for sex-
- 933        specific parental effects. *Diabetes* **45**, 1585-93 (1996).
- 934        12. Rezanian, A. et al. Reversal of diabetes with insulin-producing cells derived in vitro from human pluripotent
- 935        stem cells. *Nat. Biotechnol.* **32**, 1121-33 (2014).
- 936        13. Miyaoka, Y., Chan, A. H., & Conklin, B. R. Using Digital Polymerase Chain Reaction to Detect Single-
- 937        Nucleotide Substitutions Induced by Genome Editing. *Cold Spring Harb. Protoc.* (2016).
- 938        14. Scharfmann, R. et al. Development of a conditionally immortalized human pancreatic  $\beta$  cell line. *J. Clin.*
- 939        *Invest.* **124**, 2087-98 (2014).
- 940        15. Li, D. et al. Imaging dynamic insulin release using a fluorescent zinc indicator for monitoring induced
- 941        exocytotic release (ZIMIR). *Proc. Natl. Acad. Sci. USA* **108**, 21063-8 (2011).
- 942        16. Hastoy, B. et al. Electrophysiological properties of human  $\beta$ -cell lines EndoC- $\beta$ H1 and - $\beta$ H2 conform with
- 943        human  $\beta$ -cells. Preprint at <https://www.biorxiv.org/content/10.1101/226282v1> (2017).
- 944        17. Nicolson, T. J. et al. Insulin storage and glucose homeostasis in mice null for the granule zinc transporter
- 945        ZnT8 and studies of the type 2 diabetes-associated variants. *Diabetes* **58**, 2070-83 (2009).
- 946        18. Vinkenborg, J. L. et al. Genetically encoded FRET sensors to monitor intracellular Zn<sup>2+</sup> homeostasis. *Nat.*
- 947        *Methods* **6**, 737-40 (2009).
- 948        19. Flannick, J. et al. Exome sequencing of 20,791 cases of type 2 diabetes and 24,440 controls. *Nature* **570**, 71-
- 949        76 (2019).
- 950        20. Tamaki, M. et al. The diabetes-susceptible gene SLC30A8/ZnT8 regulates hepatic insulin clearance. *J. Clin.*
- 951        *Invest.* **123**, 4513-24 (2013).
- 952        21. Hardy, A. B. et al. Effects of high-fat diet feeding on Znt8-null mice: differences between  $\beta$ -cell and global
- 953        knockout of Znt8. *Am. J. Physiol. Endocrinol. Metab.* **302**, E1084-96 (2012).
- 954        22. Li, L., Bai, S., & Sheline, C. T. hZnT8 (Slc30a8) Transgenic Mice that Overexpress the R325W Polymorph
- 955        Have Reduced Islet Zn<sup>2+</sup> and Proinsulin Levels, Increased Glucose Tolerance After a High-Fat Diet, and
- 956        Altered Levels of Pancreatic Zinc Binding Proteins. *Diabetes* **66**, 551-559 (2017).
- 957        23. Merriman, C., Huang, Q., Rutter, G. A. & Fu, D. Lipid-tuned Zinc Transport Activity of Human ZnT8
- 958        Protein Correlates with Risk for Type-2 Diabetes. *J. Biol. Chem.* **291**, 26950-26957 (2016).
- 959        24. Gerber, P. A. et al. Hypoxia lowers SLC30A8/ZnT8 expression and free cytosolic Zn<sup>2+</sup> in pancreatic beta
- 960        cells. *Diabetologia* **57**, 1635-44 (2014).
- 961        25. Wong, W. P. et al. Exploring the Association Between Demographics, SLC30A8 Genotype, and Human
- 962        Islet Content of Zinc, Cadmium, Copper, Iron, Manganese and Nickel. *Sci. Rep.* **7**(1), 473 (2017).
- 963        26. Vergnano, A. M. et al. Zinc dynamics and action at excitatory synapses. *Neuron* **82**, 1101-14 (2014).
- 964        27. Ferrer, R., Soria, B., Dawson, C. M., Atwater, I., & Rojas, E. Effects of Zn<sup>2+</sup> on glucose-induced electrical
- 965        activity and insulin release from mouse pancreatic islets. *Am. J. Physiol.* **246**, C520-7 (1984).
- 966        28. Bloc, A., Cens, T., Cruz, H. & Dunant, Y. Zinc-induced changes in ionic currents of clonal rat pancreatic -
- 967        cells: activation of ATP-sensitive K<sup>+</sup> channels. *J. Physiol.* **529**, 723-34 (2000).

29. Zhang, Q. et al. Role of KATP channels in glucose-regulated glucagon secretion and impaired counterregulation in type 2 diabetes. *Cell Metab.* **18**, 871-82 (2013).
30. Michael, D. J. et al. Pancreatic beta-cells secrete insulin in fast- and slow-release forms. *Diabetes* **55**, 600-7 (2006).
31. Kirchhoff, K. et al. Polymorphisms in the TCF7L2, CDKAL1 and SLC30A8 genes are associated with impaired proinsulin conversion. *Diabetologia* **51**, 597-601 (2008).
32. Majithia, A. R. et al. Association of the SLC30A8 missense polymorphism R325W with proinsulin levels at baseline and after lifestyle, metformin or troglitazone intervention in the Diabetes Prevention Program. *Diabetologia* **54**, 2570-4 (2011).
33. Jainandunsing, S. et al. A stable isotope method for in vivo assessment of human insulin synthesis and secretion. *Acta. Diabetol.* **53**, 935-944 (2016).
34. Ivanova, A. et al. Age-dependent labeling and imaging of insulin secretory granules. *Diabetes* **62**, 3687-96 (2013).
35. Abecasis, G. R., Cardon, L.R. & Cookson, W.O. A general test of association for quantitative traits in nuclear families. *Am. J. Hum. Genet.* **66**, 279-92 (2000).
36. Purcell, S. et al. PLINK: a tool set for whole-genome association and population-based linkage analyses. *Am. J. Hum. Genet.* **81**, 559-75 (2007).
37. Yang, J., Lee, S. H., Goddard, M. E. & Visscher, P. M. GCTA: a tool for genome-wide complex trait analysis. *Am. J. Hum. Genet.* **88**, 76-82 (2011).
38. Isomaa, B. et al., A family history of diabetes is associated with reduced physical fitness in the Prevalence, Prediction and Prevention of Diabetes (PPP)-Botnia study. *Diabetologia* **53**, 1709-13 (2010).
39. Ahlqvist, E. et al. Novel subgroups of adult-onset diabetes and their association with outcomes: a data-driven cluster analysis of six variables. *Lancet Diabetes Endocrinol.* **6**, 361-369 (2018).
40. Lindgren, O. et al. Incretin hormone and insulin responses to oral versus intravenous lipid administration in humans. *J. Clin. Endocrinol. Metab.* **96**, 2519-24 (2011).
41. Sluiter, W. J., Erkelens, D. W., Reitsma, W. D. & Doorenbos, H. Glucose tolerance and insulin release, a mathematical approach I. Assay of the beta-cell response after oral glucose loading. *Diabetes* **25**, 241-4 (1976).
42. Mohandas, C. et al. Ethnic differences in insulin secretory function between black African and white European men with early type 2 diabetes. *Diabetes Obes. Metab.* **20**, 1678-1687 (2018).
43. Navalesi, R., Pilo, A. & Ferrannini, E. Kinetic analysis of plasma insulin disappearance in nonketotic diabetic patients and in normal subjects. A tracer study with 125I-insulin. *J. Clin. Invest.* **61**, 197-208 (1978).
44. Delaneau, O., Zagury, J. F. & Marchini, J. Improved whole-chromosome phasing for disease and population genetic studies. *Nat. Methods* **10** (1), 5-6 (2013).
45. Flannick, J. et al. Sequence data and association statistics from 12,940 type 2 diabetes cases and controls. *Sci. Data.* **4**, 170179 (2017).
46. Howie, B., Fuchsberger, C., Stephens, M., Marchini, J. & Abecasis G. R. Fast and accurate genotype imputation in genome-wide association studies through pre-phasing. *Nat. Genet.* **44**, 955-9 (2012).
47. Willer, C. J., Li, Y. & Abecasis, G. R. METAL: fast and efficient meta-analysis of genomewide association scans. *Bioinformatics* **26**, 2190-1 (2010).
48. Bonetti, S. et al. Variants of GCKR affect both  $\beta$ -cell and kidney function in patients with newly diagnosed type 2 diabetes: the Verona newly diagnosed type 2 diabetes study 2. *Diabetes Care* **34**, 1205-10 (2011).
49. van de Bunt, M. et al. Insights into islet development and biology through characterization of a human iPSC-derived endocrine pancreas model. *Islets* **8**, 83-95 (2016).
50. Cong, L. et al. Multiplex genome engineering using CRISPR/Cas systems. *Science* **339**, 819-23 (2013).
51. Krentz, N. A. J. et al. Phosphorylation of NEUROG3 Links Endocrine Differentiation to the Cell Cycle in Pancreatic Progenitors. *Dev. Cell* **41**, 129-142.e6 (2017).
52. Perez-Alcantara, M. et al. Patterns of differential gene expression in a cellular model of human islet development, and relationship to type 2 diabetes predisposition. *Diabetologia* **61**, 1614-1622 (2018).
53. Harries, L. W., Hattersley, A. T. & Ellard S. Messenger RNA transcripts of the hepatocyte nuclear factor-1alpha gene containing premature termination codons are subject to nonsense-mediated decay. *Diabetes* **53**, 500-4 (2004).
54. Dobin, A. et al. STAR: ultrafast universal RNA-seq aligner. *Bioinformatics* **29**, 15-21 (2013).
55. Harrow, J. et al. GENCODE: the reference human genome annotation for The ENCODE Project. *Genome Res.* **22**, 1760-74 (2012).
56. Smith, T., Heger, A. & Sudbery, I. UMI-tools: modeling sequencing errors in Unique Molecular Identifiers to improve quantification accuracy. *Genome Res.* **27**, 491-499 (2017).

57. Merriman, C., Li, H., Li, H. & Fu, D. Highly specific monoclonal antibodies for allosteric inhibition and immunodetection of the human pancreatic zinc transporter ZnT8. *J. Biol. Chem.* **293**, 16206-16216 (2018).
58. Ravassard, P. et al. A genetically engineered human pancreatic  $\beta$  cell line exhibiting glucose-inducible insulin secretion. *J. Clin. Invest.* **121**, 3589-97 (2011).
59. Thomsen, S. K. et al. Systematic Functional Characterization of Candidate Causal Genes for Type 2 Diabetes Risk Variants. *Diabetes* **65**, 3805-3811 (2016).
60. Chandra, V. et al. RFX6 regulates insulin secretion by modulating  $\text{Ca}^{2+}$  homeostasis in human  $\beta$  cells. *Cell Rep.* **9**, 2206-18 (2014).
61. Slepchenko, K. G. et al. Autocrine effect of  $\text{Zn}^{2+}$  on the glucose-stimulated insulin secretion. *Endocrine* **50**, 110-22 (2015).
62. Liao, Y., Smyth, G. K. & Shi, W. featureCounts: an efficient general purpose program for assigning sequence reads to genomic features. *Bioinformatics* **30**, 923-30 (2014).
63. Robinson, M. D., McCarthy, D. J. & Smyth G. K. "edgeR: a Bioconductor package for differential expression analysis of digital gene expression data." *Bioinformatics* **26**, 139-140 (2010).
64. Robinson, M. D. & Oshlack, A. A scaling normalization method for differential expression analysis of RNA-seq data. *Genome Biol.* **11**, R25 (2010).
65. Herwig, R. et al. Analyzing and interpreting genome data at the network level with ConsensusPathDB. *Nat. Protoc.* **11**, 1889-907 (2016).
66. Mootha, V. K. et al. PGC-1 $\alpha$ -responsive genes involved in oxidative phosphorylation are coordinately downregulated in human diabetes. *Nat. Genet.* **34**, 267-73 (2003).
67. Asfari, M. et al. Establishment of 2-mercaptoethanol-dependent differentiated insulin-secreting cell lines. *Endocrinology* **130**, 167-78 (1992).
68. Ramracheya, R. et al. Membrane potential-dependent inactivation of voltage-gated ion channels in  $\alpha$ -cells inhibits glucagon secretion from human islets. *Diabetes* **59**, 2198-208 (2010).
69. Ottosson-Laakso, E. et al. Glucose-Induced Changes in Gene Expression in Human Pancreatic Islets: Causes or Consequences of Chronic Hyperglycemia. *Diabetes* **66**, 3013-3028 (2017).
70. Fadista, J. et al. Global genomic and transcriptomic analysis of human pancreatic islets reveals novel genes influencing glucose metabolism. *Proc. Natl. Acad. Sci. U S A* **111**, 13924-9 (2014).
71. Rosengren, A. H. et al. Overexpression of  $\alpha 2A$ -adrenergic receptors contributes to type 2 diabetes. *Science* **327**, 217-20 (2010).
72. Taneera, J. et al. Identification of novel genes for glucose metabolism based upon expression pattern in human islets and effect on insulin secretion and glycemia. *Hum. Mol. Genet.* **24**, 1945-55 (2015).

## URLs

GCTA, <http://cns.genomics.com/software/gcta>;  
 SHAPEIT, [http://mathgen.stats.ox.ac.uk/genetics\\_software/shapeit/shapeit.html](http://mathgen.stats.ox.ac.uk/genetics_software/shapeit/shapeit.html),  
 IMPUTE2, [http://mathgen.stats.ox.ac.uk/impute/impute\\_v2.html](http://mathgen.stats.ox.ac.uk/impute/impute_v2.html)  
 ConsensusPathDB, <http://cpdb.molgen.mpg.de/>  
 PLINK, <http://zzz.bwh.harvard.edu/plink/contact.shtml#cite>  
 METAL, <http://www.sph.umich.edu/csg/abecasis/metal/>

## Acknowledgements

We thank the Botnia Study Group for recruiting and studying the participants, Jens Juul Holst for measuring GLP-1 concentrations, and Linda Boselli, PhD, for carrying out mathematical modelling of the OGTT studies. We thank Dr. Dax Fu (Department of Physiology, The Johns Hopkins School of Medicine, Baltimore, Maryland) for providing monoclonal anti-ZnT8 antibody. We thank Dr Wen-hong Li (Departments of Cell Biology and of Biochemistry, University of Texas Southwestern Medical Center, Dallas) for providing zinc probe ZIMIR. We thank Erqian Na for her help with the mouse immunohistochemistry and histology, and Catherine Green and the Chromosome Dynamics & Genome Engineering Cores at the Wellcome Centre for Human Genetics for support with karyotyping and genome editing (funded by the Wellcome Trust grant 203141). We thank the Sequencing Unit core facility at FIMM Technology Centre supported by University of Helsinki and Biocenter Finland. The Botnia and The PPP-Botnia studies (L.G., T.T.) have been financially



supported by grants from Folkhälsan Research Foundation, the Sigrid Juselius Foundation, The Academy of Finland (grants no. 263401, 267882, 312063 to LG, 312072 to TT), Nordic Center of Excellence in Disease Genetics, EU (EXGENESIS, EUFP7-MOSAIC FP7-600914), Ollqvist Foundation, Swedish Cultural Foundation in Finland, Finnish Diabetes Research Foundation, Foundation for Life and Health in Finland, Signe and Ane Gyllenberg Foundation, Finnish Medical Society, Paavo Nurmi Foundation, Helsinki University Central Hospital Research Foundation, Perklén Foundation, Närpes Health Care Foundation and Ahokas Foundation, as well as by the Ministry of Education in Finland, Municipal Health Care Center and Hospital in Jakobstad and Health Care Centers in Vasa, Närpes and Korsholm. The work described in this paper has been supported with funding from collaborative agreements with Pfizer Inc., as well as with Regeneron Genetics Center LLC. J.L. was supported by Vinnova - Sweden's Innovation Agency (2015-01549), Swedish Diabetes Foundation, Albert Pahlsson Foundation, Hjelt Foundations, Crafoord Foundation, Royal Physiographic Society in Lund, Swedish Foundation for Strategic Research (IRC15-0067), Swedish Research council (2009-1039, Strategic research area Exodiab); E.A. by Crafoord Foundation, Pahlsson Foundation, Swedish Research Council (Dnr: 2017-02688); O.H. by Lund University Diabetes Center, ALF, Crafoord foundation, Novo Nordisk foundation, Magnus Bergvall foundation, Pahlsson foundation, Diabetes Wellness and Swedish Diabetes Research Foundation; R.C.B. by Italian Ministry of University and Research (PRIN 2015373Z39\_004) and University of Parma Research Funds; G.R. by a Wellcome Trust Senior Investigator Award (WT098424AIA), MRC Programme grants (MR/R022259/1, MR/J0003042/1, MR/L020149/1) and Experimental Challenge Grant (DIVA, MR/L02036X/1), MRC (MR/N00275X/1), Diabetes UK (BDA/11/0004210, BDA/15/0005275, BDA 16/0005485) and Imperial Confidence in Concept (ICiC) grants, and a Royal Society Wolfson Research Merit Award. ALG is a Wellcome Trust Senior Fellow in Basic Biomedical Science. M.I.M. and P.R. are Wellcome Senior Investigators. This work was funded in Oxford by the Wellcome Trust (095101 [ALG], 200837 [A.L.G.], 098381 [M.I.M.], 106130 [A.L.G., M.I.M.], 203141 [A.L.G., B.D., M.I.M.], 203141 [M.I.M.], 090531 [P.R.]), Medical Research Council (MR/L020149/1) [M.I.M., A.L.G., P.R.], European Union Horizon 2020 Programme (T2D Systems) [A.L.G.], and NIH (U01-DK105535; U01-DK085545) [M.I.M., A.L.G.]. The research was funded by the National Institute for Health Research (NIHR) Oxford Biomedical Research Centre (BRC) [A.L.G., M.I.M., P.R.]. The views expressed are those of the author(s) and not necessarily those of the NHS, the NIHR or the Department of Health.

#### Author Contributions

M.L., L.S., T.T. and L.G. conducted the human study; E.A., O.H., A.B., O.P.D. and J.F. analyzed the genotype data ; M.L., O.P.D., M.T., E.B., R.C.B, T.T. and L.G. analyzed the human data; B.H., A.G, N.L.B., S.K.T., M.vD.B., V.C., O.P.D., T.O. and A.L.G. characterized the Human beta-cell model; N.A.J.K., F.A., N.L.B., B.C., D.M., P.K., B.D., O.P.D., A.S., M.I.M. and A.L.G. characterized the human IPS cell derived model; U.K., R.P., O.P.D., B.H., A.J.P., I.S., R.R., I.A., P.R., M.I.M. and A.L.G. characterized the human islets; S.K., D.G. and J.G. characterized the *Slc30a8* p.Arg138\* mice; D.J., J.O.L., P.C., A.T., R.C., A-M.R., J.B. and G.R. characterized the rat insulinoma cell-line; M.I.M., A.L.G., T.T. and L.G. supervised the project; O.P.D., M.L., B.H., N.A.J.K., S.K., P.R., A.L.G., T.T., and L.G. wrote the manuscript; all authors revised the manuscript.

#### Materials & Correspondence

Correspondence and requests for materials should be addressed to L.G. (leif.groop@med.lu.se).

1131 **Competing interests**

1132  
1133 L.G. has received research funding from Pfizer Inc, Regeneron Pharmaceuticals, Eli Lilly and Astra  
1134 Zeneca. N.L.B. and M.vD.B are now employees of Novo Nordisk, although all experimental work  
1135 was carried out under employment at the University of Oxford. ALG has received honoraria from  
1136 Novo Nordisk and Merck. MIM serves on advisory panels for Pfizer, Novo Nordisk, Zoe Global;  
1137 has received honoraria from Pfizer, Novo Nordisk and Eli Lilly; has stock options in Zoe Global;  
1138 has received research funding from Abbvie, Astra Zeneca, Boehringer Ingelheim, Eli Lilly, Janssen,  
1139 Merck, Novo Nordisk, Pfizer, Roche, Sanofi Aventis, Servier, Takeda. [GAR is a consultant for Sun](#)  
1140 [Pharma and has received grant funding from Servier. J.O.L. has received research funding from](#)  
1141 [Pfizer Inc and Novo Nordisk A/S.](#)  
1142  
1143  
1144  
1145  
1146  
1147  
1148  
1149  
1150  
1151  
1152  
1153  
1154  
1155  
1156  
1157  
1158  
1159  
1160  
1161  
1162  
1163  
1164  
1165  
1166  
1167  
1168  
1169  
1170  
1171  
1172  
1173  
1174  
1175  
1176  
1177  
1178  
1179  
1180  
1181  
1182  
1183  
1184  
1185  
1186  
1187  
1188

## Figure legends

### Fig. 1: A flow-chart describing the study design.

OGTT; oral glucose tolerance test, IVGTT; intravenous glucose tolerance test, GTT; glucose tolerance test

**a**, The study design including various model systems (left panels), methods (middle panels) and the purpose of these experiments (right panels).

**b**, Detailed description of the human *in vivo* studies, including a genotype-based recall study for p.Arg138\* carriers and their relatives for metabolic studies.

### Fig. 2: SLC30A8-p.Arg138\* enhances insulin secretion and proinsulin processing during test meal.

Association of *SLC30A8* p.Arg138\* and p.Trp325Arg variants with **a**, plasma glucose **b**, serum insulin **c**, insulin/glucose ratio **d**, proinsulin/C-peptide ratio and **e**, proinsulin/insulin ratio during test meal. *Left panel*: Carriers (red, n=54) vs. non-carriers (black, n=47) of p.Arg138\*. *Middle panel*: Carriers of p.Arg138\* (red, n=54) vs Arg138Arg having the common risk variant p.Arg325 (blue, n=31). *Right panel*: Carriers of p.Trp325Trp (grey, n=16) vs. p.Arg325 (blue, n=31). Data are Mean  $\pm$  SEM. \*P values (\*p<0.05, \*\*p<0.01) for family-based association (using QTDT<sup>35</sup>) after 100,000 permutations, adjusted for age, sex and BMI for left panel and age, sex, BMI and genotype of p.Trp325Arg for middle panel. #P value (#p<0.05) calculated using family-based QFAM test using 100,000 permutations as implemented in PLINK<sup>36</sup>.

### Fig. 3: SLC30A8 p.Arg138\* and p.Trp325 enhance insulin secretion during OGTT.

Association of *SLC30A8* p.Arg138\* and p.Trp325Arg with **a**, plasma glucose **b**, serum insulin **c**, insulin/glucose ratio during an oral glucose tolerance test (OGTT). *Left panel*: Carriers (red, n=34-35) vs. non-carriers (black, n=7954-8141) of p.Arg138\*. *Middle panel*: Carriers of p.Arg138\* (red, n=34-35) vs. p.Arg138Arg having the common risk variant p.Arg325 (blue, n=6728-6893). *Right panel*: Carriers of p.Trp325Trp (grey n=1226-1248) vs. p.Arg325 (blue, n=6728-6893). Data are shown as Mean  $\pm$ SEM. \*P values (\*p < 0.05, \*\*p< 0.01) for additive effect were calculated using mixed model adjusting for genetic relationship, age, sex, BMI and additionally genotype of p.Trp325Arg only for middle panel as implemented in GCTA<sup>37</sup>. Y-axis: note truncation ( $\wedge$ ) and different scale in the right panel.

**Fig. 4: Beta like cells derived from SLC30A8-p.Arg138\* iPSCs display haploinsufficiency of SLC30A8.**

**a-c**, Characterization of *SLC30A8* expression at the (a) mRNA and (b-c) protein level in cells heterozygous for *SLC30A8*-p.Arg138\* or homozygous for *SLC30A8*-p.Lys34Serfs50\*. Gene expression data normalized to *TBP* and expressed as fold change relative to p.Arg138Arg control (n=7-13 wells from three differentiations). **d-e**, Allele-specific expression (ASE) of p.Arg138Arg (black bar) and p.Arg138\* (red bar) in clone A3 or clone B1 derived cells using (d) Digital Droplet PCR based probes also validated by (e) target *SLC30A8* mRNA sequencing of p.Arg138\* clones (n=number of unique sequencing reads for each allele). **f-g**, Allele-specific expression of p.Arg138Arg (black bar) and p.Arg138\* (red bar) in f, clone A3 and g, clone B1 derived cells treated with DMSO (Dimethyl sulfoxide) or cycloheximide (CHX) for four hours. ASE data (Mean±SEM) determined by Digital Droplet PCR were presented as fold change relative to p.Arg138Arg transcript (d, n=5-7 wells from three differentiations) or to DMSO control (f-g, n=9 wells from two differentiation). \*p<0.05, \*\*p<0.01, \*\*\*\*p<0.0001 one-way ANOVA Holm-Sidak's multiple comparison test (a) or one-sample t-test (d, f and g) or binominal test considering 0.5 as expected probability (e).

**Fig. 5: SLC30A8 knock down leads to enhanced insulin secretion, proinsulin processing and cell viability in the human pancreatic EndoC-βh1 cells.**

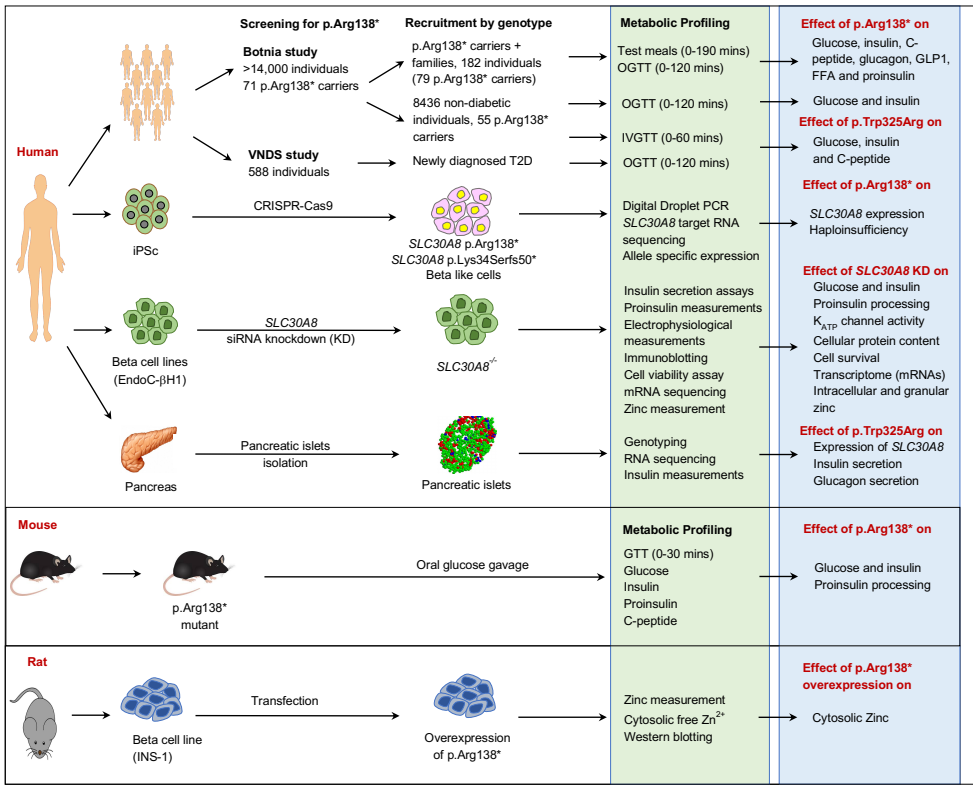
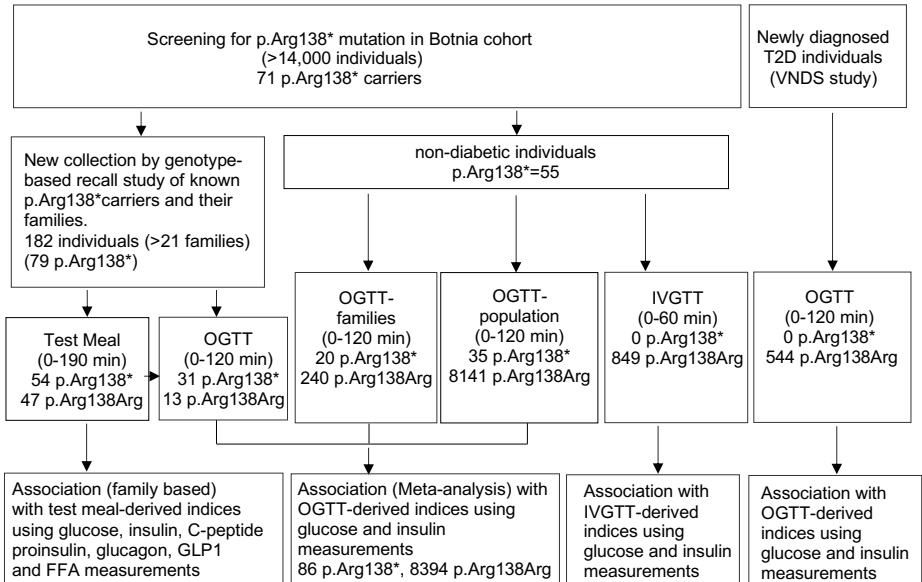
**a-b**, Effect of siRNA mediated knock down (KD) on *SLC30A8* mRNAs and protein. **c**, Measurement of intracellular zinc using zinc-specific fluorescent dye Zinpyr-1. **d-i**, Effect of KD on (d) insulin secretion stimulated by glucose and K<sub>ATP</sub> channel regulators (as labelled), (e) insulin content, (f) K<sub>ATP</sub> channel conductance (Gm), (g) cell size, (h) expression of K<sub>ATP</sub> channel subunits, (i) insulin secretion stimulated by KCL and high glucose. **j-p**, Effect of KD on proinsulin processing estimated by proinsulin/insulin ratio (j), proinsulin concentration (k) and protein expression of proinsulin processing enzymes PC1/3, CPE and PC2 (immunoblot- l and p, densitometry- m, n and o). **q-s**, Effect of KD on basal (5.5 mM glucose) AKT phosphorylation (q, densitometry, r, immunoblot; phospho-AKT-Ser473, total AKT) and cell viability under ER stress (s, MTT assay, 10 µg/ml tunicamycin, DMSO as vehicle control). Data are shown as Mean ±SEM (n=3-10). \*p<0.05, \*\*p<0.01, \*\*\*p<0.001 using Mann-Whitney test; #p<0.05 one-sample t-test; d (Bonferroni multiple correction for 4 conditions).

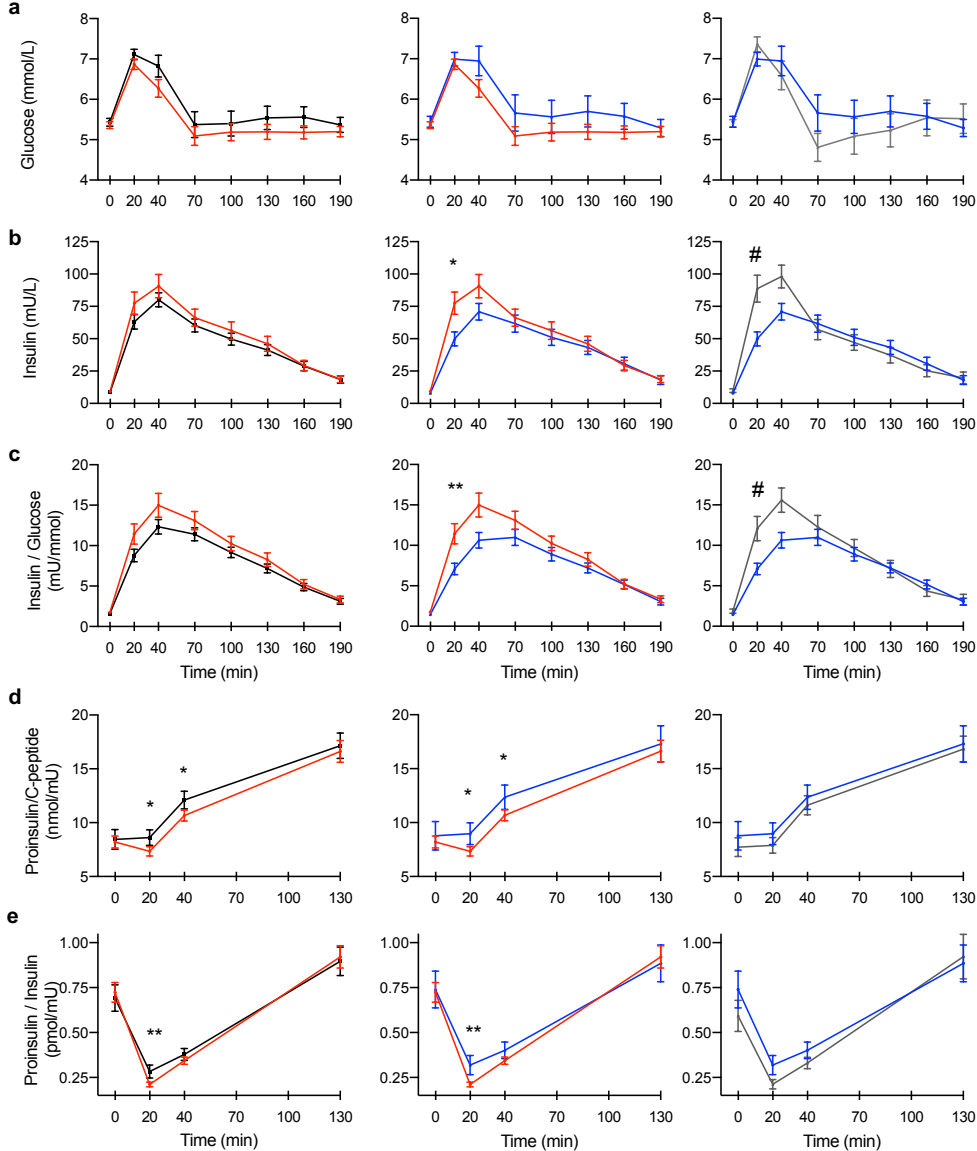
**Fig. 6: Male p.Arg138\* mice on high-fat diet show enhanced insulin secretion and proinsulin processing.**

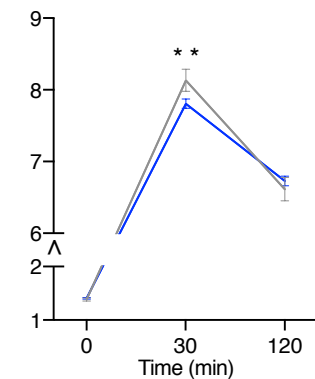
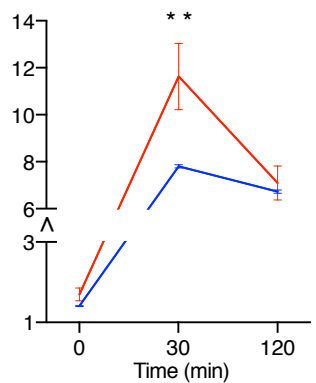
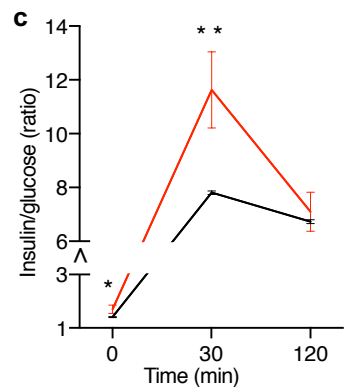
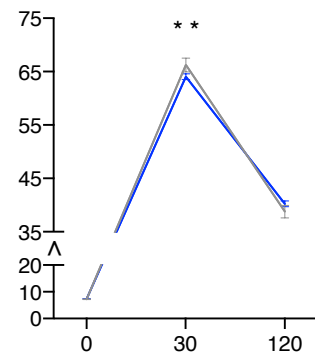
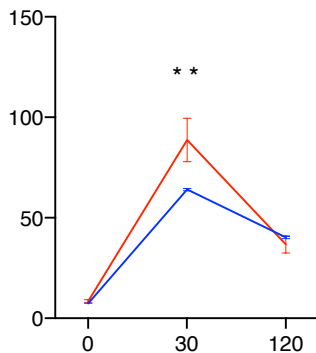
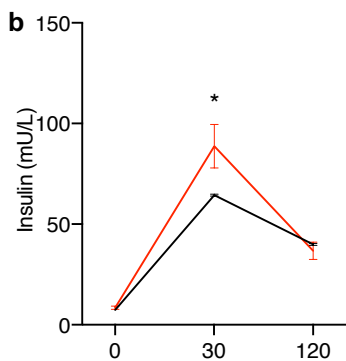
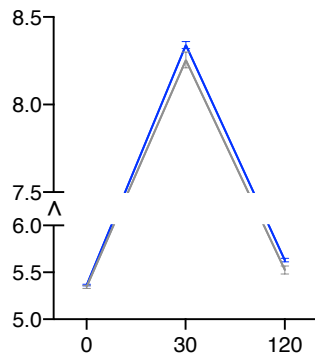
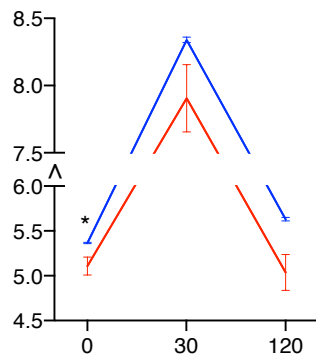
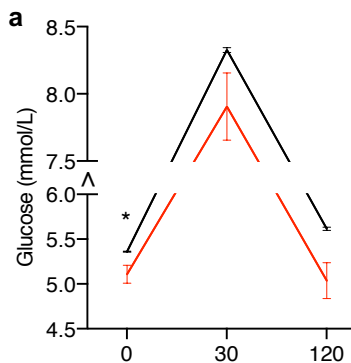
**a**, Body weight, circulating **b**, glucose **c**, insulin **d**, proinsulin (\*p=0.011) **e**, C-peptide **f**, proinsulin/insulin ratio (\*p=0.0004) **g**, proinsulin/C-peptide ratio (\*p<0.0001) and **h**, insulin/C-peptide ratio in fasted WT and p.Arg138\* mice (n= 10 WT, 17 p.Arg138\*) after 20 weeks on HFD. **i**, Insulin response to oral glucose (2g/kg) exposure (n=5 WT, 9 p.Arg138\*) after 30 weeks on HFD. **j**, Blood glucose levels over time after **j**, oral glucose (2g/kg) exposure (n=5 WT, 11 p.Arg138\*) after 29 weeks on HFD and **k**, interperitoneal injection of insulin (1.75 U/kg) after 28 weeks on HFD (n=11 WT, 13 p.Arg138\*). \*p<0.05, \*\*\*p<0.001, \*\*\*\*p<0.0001 using Mann Whitney test; #p<0.05, ##p<0.01 using two-way Anova and Sidak's multiple comparison test.

**Fig. 7: SLC30A8- p.Trp325 leads to enhanced insulin secretion in human islets.**

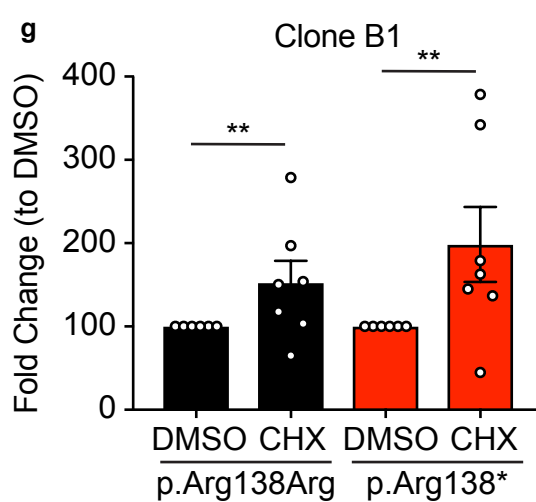
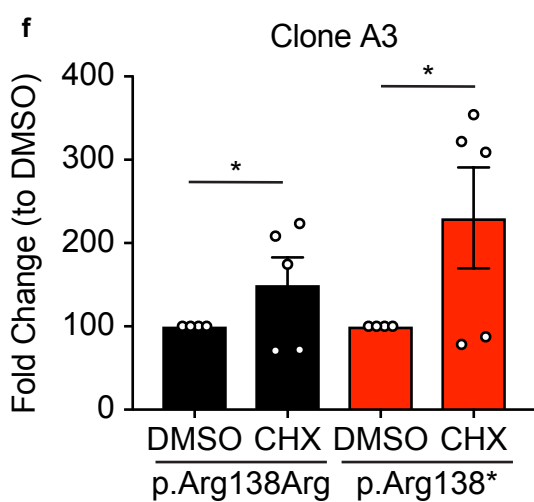
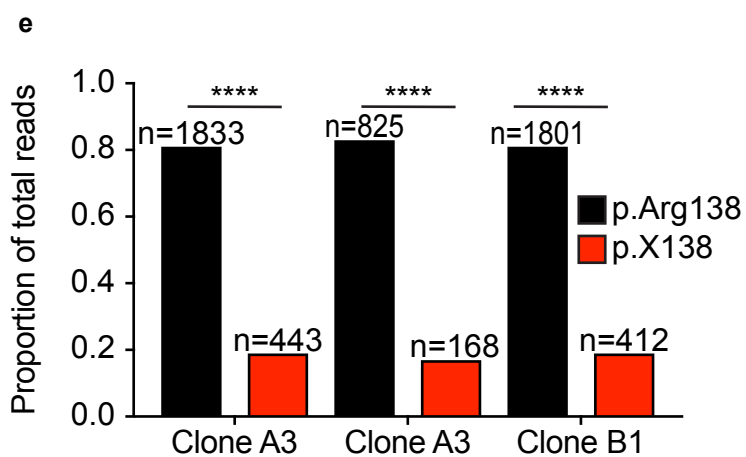
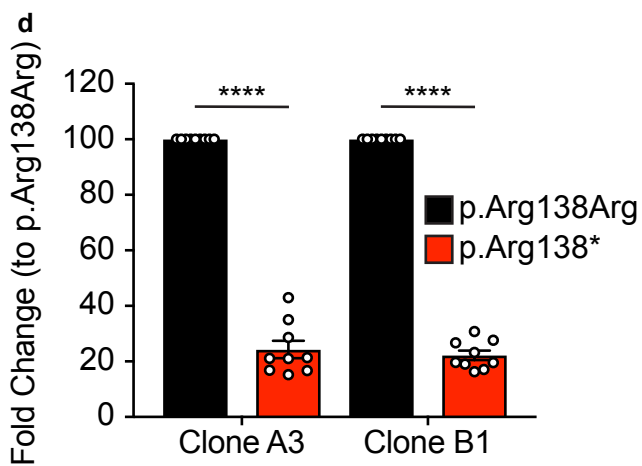
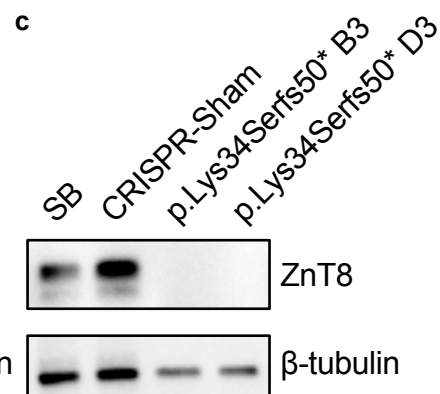
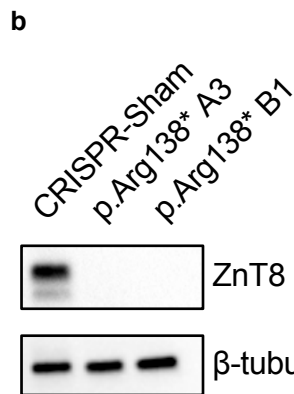
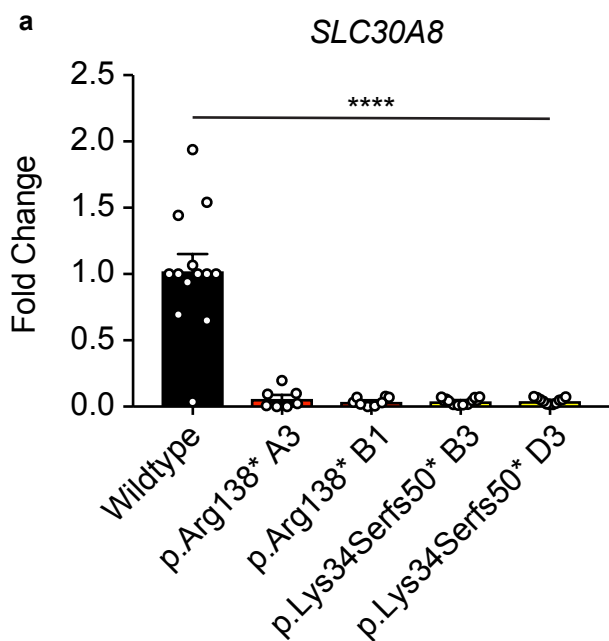
Experiments have been performed in two different centers: LUDC (**a**, **b**, **g**, **h**, **i** and **j**) and Oxford (**c**, **d**, **e** and **f**). **a**, Effect of p.Trp325Arg genotype on static insulin secretion in presence of low and high glucose stimulatory conditions. **b**, Effect of p.Trp325Arg genotype on static insulin secretion in presence of low or high glucose and KCL. **c-d**, Effect of p.Trp325Arg genotype on static insulin secretion in (**c**) sub-maximal stimulatory conditions (6mM glucose) and their (**d**) insulin contents. **e**, Static glucagon response to glucose and **f**, glucagon content at basal glucose. **g-h**, Correlation of SLC30A8 expression with candidate genes of *INS*, *GCG*, proinsulin processing genes and  $K_{ATP}$  channel subunits genes among (**g**) p.Arg325Arg individuals and (**h**) p.Trp325 carriers and effect of p.Trp325Arg genotype (p.Arg325Arg=65, p.Trp325Arg=63 and p.Trp325Trp=11) on expression (cpm=log2 of counts per million) of (**i**) SLC30A8 and (**j**) other candidate genes. Data are Mean  $\pm$ SEM; Glu- glucose. \*p<0.05, \*\*\*p<0.0001 using Mann-Whitney test (**b**, **c**, **d**, **e** and **f**) or Spearman correlation coefficient (r) with two-tailed p values (**g** and **h**). Three genotype comparison (**a**, **i** and **j**) by linear regression using additive effect adjusting for age, sex and islet purity as implemented in PLINK<sup>36</sup>.

**a****b**

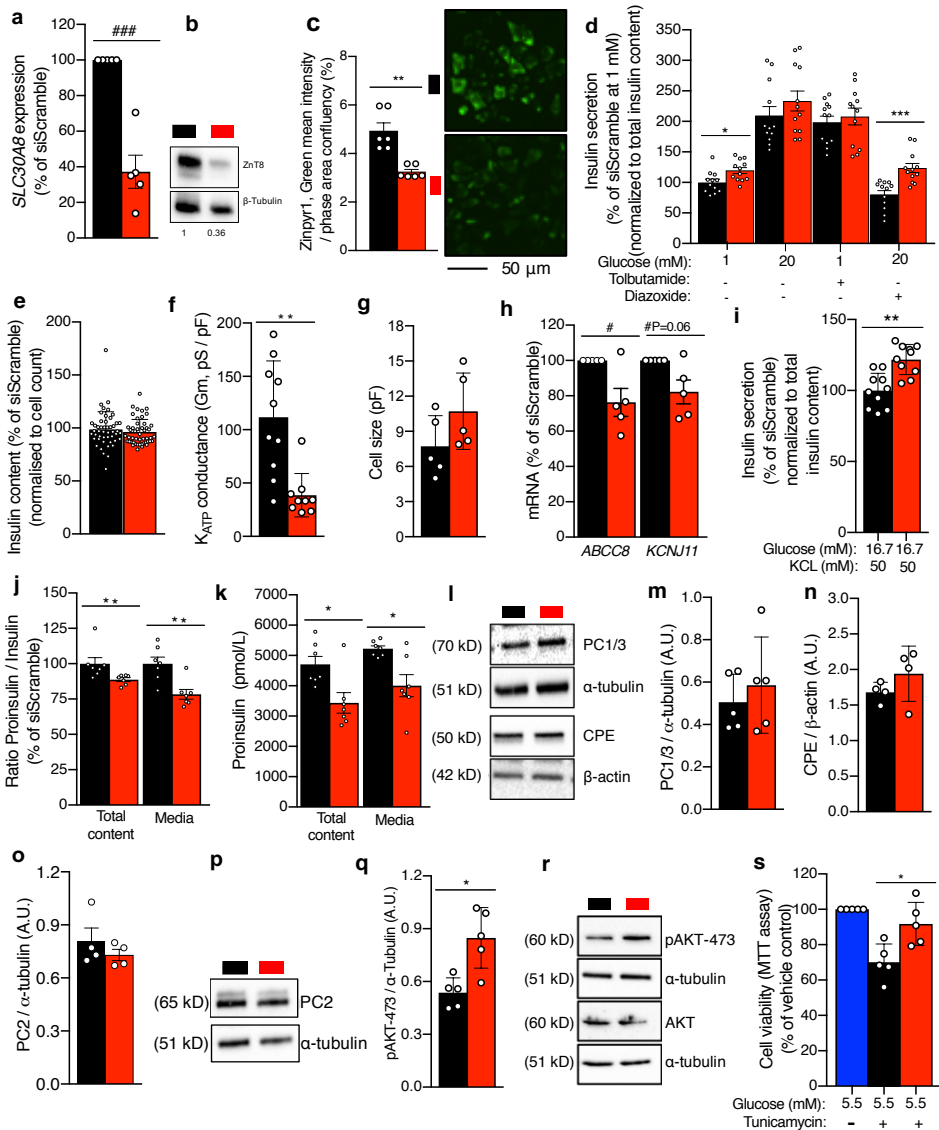


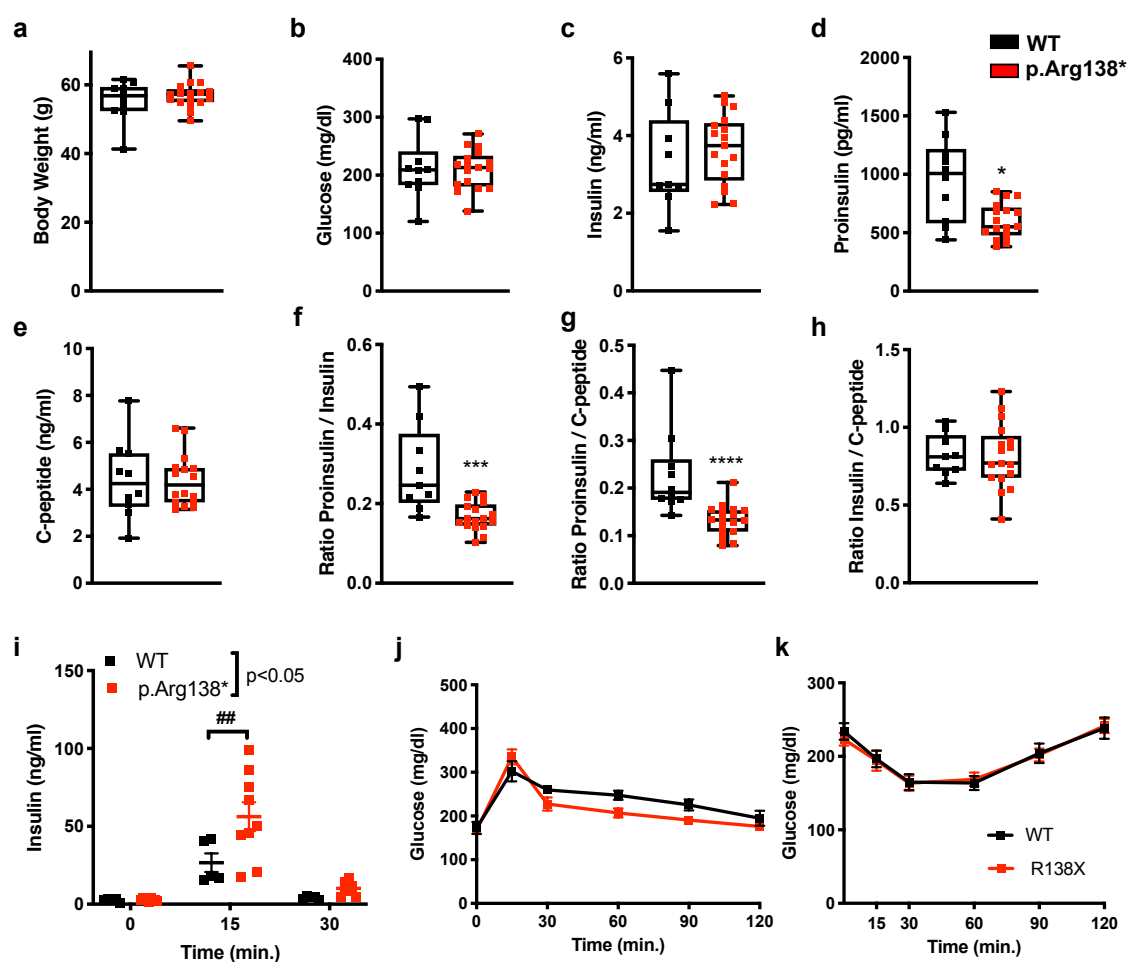






■ siScramble ■ siSLC30A8





■ p.Arg325Arg

■ p.Trp325Arg

■ p.Trp325Trp

